ABSTRACT

Creep tests were carried out on compression test specimens of 99.999 per cent pure zinc single crystals oriented for basal slip. Measurements of initial dislocation densities were made and changes in the dislocation density after testing were observed. The change in dislocation density for a given strain was found to depend on the density of grown-in dislocations. The effect of the non-basal dislocations in controlling the yield stress of a crystal was confirmed, while the density of basal dislocations was found to have no direct influence on this stress.

A marked decrease in the creep rate was observed after an initial primary stage, followed by subsequent recovery.

The number of active slip planes in a specimen was found to be directly proportional to the applied stress in the test range. This relationship offered an explanation of the effect of a stress increase on deformation processes not thermally activated.

THE MICROSTRUCTURE OF ZINC SINGLE CRYSTALS DURING CREEP

by

Kenneth Marc Jassby

B.Eng., McGill University, 1965

A THESIS SUBMITTED IN PARTIAL FULFILMENT

OF THE REQUIREMENTS FOR THE DEGREE OF

Master of Engineering

in the Department

of

Mechanical Engineering

McGill University

September, 1966.

ABSTRACT

Creep tests were carried out on compression test specimens of 99.999 per cent pure zinc single crystals oriented for basal slip. Measurements of initial dislocation densities were made and changes in the dislocation density after testing were observed. The change in dislocation density for a given strain was found to depend on the density of grown-in dislocations. The effect of the non-basal dislocations in controlling the yield stress of a crystal was confirmed, while the density of basal dislocations was found to have no direct influence on this stress.

A marked decrease in the creep rate was observed after an initial primary stage, followed by subsequent recovery.

The number of active slip planes in a specimen was found to be directly proportional to the applied stress in the test range. This relationship offered an explanation of the effect of a stress increase on deformation processes not thermally activated.

TABLE OF CONTENTS

LIST OF TABLES

ACKNOWLEDGEMENTS

The author wishes to thank Dr. D.R. Axelrad for his supervision of the work described in this thesis, and for his many helpful comments and suggestions.

The author is grateful to Dr. J.J. Jonas for his continuing interest in the project and for his useful criticisms of the interpretation of the experimental results.

The author would like to thank Mr. E. Jones for his generous assistance in the assembly of the creep furnace and in the design and fabrication of the auxiliary test equipment. Thanks are also due to Mr. L. Vroomen for providing many useful ideas as pertained to the laboratory work. Technical assistance extended to the author by Professor P. Zomber-Murray and Mr. J. Kelly is gratefully acknowledged.

The author is indebted to the National Research Council of Canada for the scholarship held during the course of this work. He would like to express his appreciaion to Professor W. Bruce for making available a special summer Research Grant.

The author wishes to express his appreciation to Miss M. Herman for her help in the numerical tabulations and calculations and to Mr. A. Jassby for reproducing some of the figures.

Finally, it is a pleasure for the author to thank Mrs. S. Richards for typing the thesis.

Chapter I

INTRODUCTION

Creep is defined as the time-dependent deformation of materials that occurs under constant stress and temperature. In the earliest investigations of this phenomenon in both single and polycrystalline materials attempts have been made to characterize the process by generalized equations or time laws. In a review of these laws, Cottrell (1952-1953) found that many of the experimental creep curves could be fitted by the equation :

$$\dot{\gamma} = a t^{-n}$$

where $\dot{\gamma}$ = strain rate

t = time

a = constant for a single test

n = constant for a single test

It was found that a , n varied from specimen to specimen. Consequently many attempts were made to evaluate the dependence of a and n on the applied stress and temperature. The investigators determined three distinct regions of temperature:

(1) low temperature ($0 < T < 0.25 T_m$) where $n = 1$.

(2) intermediate temperature ($0.25 T_m < T < 0.5 T_m$) where $0 < n < 1$

(3) high temperature ($0.5 T_m < T < T_m$) where $n = 0$.

The three regions thus termed logarithmic creep, parabolic creep, and steady-state creep, respectively are summarized by Conrad (1961). The first work dealing with the forms of the creep curves lead to the well known exhaustion theory of creep proposed by Kauzmann (see also Cottrell (1953)) and used

abstract concepts in order to explain the temperature and stress-dependence of α and n. This theory, and the formal theories to follow, were based on the idea that thermal fluctuations aid the applied stress to cause flow in overcoming internal barriers.

The first theory of work-hardening based on dislocations is due to Taylor (1934). He postulated that dislocations were constantly being created while the substance was undergoing deformation and that they moved a certain distance before they were arrested. Mott (1952) extended this theory by proposing that the strain hardening could be accounted for by the internal stress field of the generated dislocations.

Most of the present theories lead to an equation of the type:

$$\dot{\gamma} = c(T,\sigma)\exp-\left[\frac{u(T,\sigma)}{KT}\right]$$

where T = temperature

σ = applied resolved shear stress

K = Boltzmann's constant

$u(T,\sigma)$ = activation energy associated with the flow.

The mathematical forms of the strain-rate equations for the various theories differ essentially in the relation between the activation energy and the applied stress and temperature. Schoeck (1961), Conrad (1961) and Friedel (1964) have made comprehensive evaluations of the theories applicable at various stress and temperature levels.

Another approach to the understanding of work-hardening and creep has been to consider the parameters involved in the basic strain-rate equation for slip on one plane, separately, viz:

$$\dot{\gamma} = N\bar{v}b$$

where N = total length of moving dislocation line per unit volume

$\bar{v}$ = average velocity of the moving dislocations

b = magnitude of the Burgers vector of the mobile dislocations.

Johnston and Gilman (1959) measured dislocation velocities directly in Lithium fluoride by using an etch pit technique. Since then, dislocation velocities have been measured in several other crystals (see also Adams et al (1965b)). However, the proportion of dislocation loops that are mobile in a crystal undergoing deformation has not been determined as yet experimentally in bulk specimens.

The present experimental investigation is an attempt to examine by using an etch pit technique, the re-arrangement and multiplication of dislocations during the creep of 99.999 per cent pure zinc single crystals with different values of grown-in dislocation densities. The aim of this work is to provide further knowledge toward an understanding of the mode of work-hardening in pure zinc crystals.

Chapter II

EXPERIMENTAL TECHNIQUES

a) Specimen Preparation

The test specimens were made from HP grade zinc of 99.999 per cent purity, obtained from COMINCO LIMITED, Trail, B.C. According to the supplier, iron (0.0003 per cent) and lead (0.0001 per cent) were the major impurities.

Single crystals of dimensions 6.00" x 0.55" x 0.55" were prepared by seeded growth in a graphite mould placed inside a horizontal travelling furnace. The furnace moved at a rate of 5 cm/hr. The basal plane of each crystal was parallel to the growth direction within $\pm$ 0.5° and at an angle of 45 $\pm$ 0.5° to the vertical walls of the mould, while the $\langle \bar{1}2\bar{1}0 \rangle$ basal slip direction was perpendicular to the growth direction within $\pm$ 1° (see Figure 1).

The first third of each crystal was used for the purpose of test specimens. This part (approximately 2 ins. length) of the crystal was sawed into 0.56 inch sections using an acid-cutting machine; the cutting edge was a cotton thread wet with 16N nitric acid. These cutting operations resulted in surfaces with irregularities less than 2×10^{-3} inch in height.

The loading surfaces of the specimens were the two planes of the crystal parallel to the vertical walls of the graphite mould. By proper machining of the mould, it was possible to obtain these surfaces parallel to within 0.1°.

The cut surfaces of each specimen were chemically polished on a slowly turning lucite disk covered with a thin film of 6N nitric acid. The polishing operation removed approximately 4×10^{-3} inch of material from each face and left them parallel to within 1°. During the polishing the remaining four surfaces were masked with tape to retain a flat surface.

The crystallographic orientation of the test specimens is shown in Figure 2.

The maximum possible basal resolved shear stress uncertainly resulting from the ~~uncertainties~~ uncertainty in the angles θ_1 , θ_2 was less than one per cent.

b) Test Equipment

1. Creep Furnace.

Creep tests were carried out in a high temperature furnace employing graphite rods as heating resistors. A complete description of the creep furnace is given by Axelrad (1962), (1965).

The compressive load train is illustrated in Figure 3. Calibrated weights were placed on the flat upper surface of the loading rod. The load was transmitted to the test specimen through the silicon carbide upper push rod and tungsten platen. Thus the total load supported by the specimen during creep testing consisted of the upper load train plus calibrated weights, less any frictional losses. These losses were determined by measuring deflections under loading of a calibrated spring placed between the two platens. The frictional losses proved negligible.

To insert a test specimen into the furnace, the sliding plate was removed and the lower push road extracted from the furnace through the bottom.

The specimen was placed between marked lines on the lower tungsten platen and the lower push rod was then re-inserted into the furnace. To prepare the load for the commencement of a test, the upper loading fixture was lowered to the level of the specimen's upper surface, and fixed there by the load-application device (Figure 4). Thereupon the clamping screw was released to allow the load to rest wholly on the test specimen.

2. Strain Measuring Device.

A Starrett Model No. 25-231 dial gauge sensitive to 2.5×10^{-5} inches and connected to a 1:2 lever arm was used to measure vertical displacements of the loading rod. This unit provided a displacement sensitivity of 1.3×10^{-5} inches.

3. Temperature Control Circuit.

A temperature control unit was employed which maintained the specimen temperature within $\pm 2^{\circ}C$ of any set-point temperature.

A general schematic of the temperature control system is shown in Figure 5.

The chromel-alumel thermocouple located at the specimen's surface transmitted a millivolt signal, proportional to the specimen temperature, which actuated the pen in the Honeywell Electronik 15 strip chart recorder.

The 200 Ω retransmitting slidewire attached to the pen drive system was wired between two dropping resistors across a 40 volt power supply. A process variable voltage signal PV, proportional to the thermocouple signal, was therefore available for the control system from the wiper on this slidewire.

For the automatic control of the furnace temperature, a "set point" signal, SP, against which a process variable signal, PV, could be compared, was provided to the controller by means of a 10 turn set point potentiometer. The set point was adjusted on a dial calibrated from 0 to 10, equivalent to 0 to 100 per cent of scale on the strip chart recorder.

The controller was a three-mode Honeywell Electro-O-Volt Model which compared the SP, PV signals to produce a difference or the error signal SP, PV, in millivolts.

This signal actuated the silicon controlled rectifier power modulator, which controlled the power to the heating element. Using this system it was possible to maintain steady-state temperatures with a fluctuation of less than $\pm$ 2°C.

In order to measure any temperature variation around the periphery of the test specimen, six chromel-alumel thermo-couples with 2 x 10^{-3} inch flattened beads were located at equal intervals around the specimen. The thermocouples were connected to a Honeywell 12-channel Electronik recorder and the temperature of each thermocouple was recorded every 9 seconds. Temperatures were measured to the nearest 2.5°C. No variation in temperature around the specimen could be detected during any test.

c) Test Procedures

1. Annealing of Test Specimens.

Prior to testing, all test specimens were annealed at 360°C for 8 hours in a purified nitrogen atmosphere.

2. Observation of Dislocations.

Dislocation etch pits on both $(10\bar{1}0)$* prism planes of each test specimen were counted before and after the creep test. A minimum of 6 photomicrographs was taken from each plane and a qualitative description of the number and distribution of low-angle boundaries was made. In addition, following the photography after the creep test, each specimen was cleaved on the basal plane. This was done by cooling the crystal to the temperature of liquid air at a rate of about 4°C per minute and thereupon cleaving it with a razor blade tapped lightly with a hammer. At least seven photomicrographs were taken of each cleaved surface.

To reveal dislocation etch pits on $(10\bar{1}0)$ surfaces, an etch pit technique, developed by Brandt et al (1963) was found suitable. Mercury, in the form of a $Hg(NO_3)_2$ solution, was introduced to the polished specimen surface, where it concentrated at the individual dislocation centres to produce etch pits.

Etch pits on the (0001) basal plane were revealed by an etchant developed by Rosenbaum and Saffren (1961) and Rosenbaum (1961). Of the several possible etchants which revealed pits, the one used in these experiments was 48 per cent HBr in ethanol. This etchant produced hexagonal pits with sides parallel to the $\langle\bar{1}2\bar{1}0\rangle$ directions (see Figure 9).

* One plane is actually $(\bar{1}010)$.

The dislocation density on each surface was calculated by counting etch pits on the photomicrographs. On the photomicrographs of the $(10\bar{1}0)$ surfaces before testing and of the (0001) planes, all the etch pits were counted. For the $(10\bar{1}0)$ surfaces after the creep test, etch pits were counted inside a one-centimeter square placed on each picture. At least twenty-five of these tabulations were made from each photomicrograph.

The specimens were etched immediately after annealing and the first set of $(10\bar{1}0)$ plane photomicrographs was taken. The crystals were then placed in a vacuum of 2.3×10^{-5} mm.Hg. at room temperature for twelve hours to remove from the surface as much of the etchant as possible. Subsequent repolishing of about four minutes reproduced highly reflective $(10\bar{1}0)$ planes. Great care was taken in handling the specimens during these operations so as to avoid the introduction of new dislocations into them. After creep testing, the $(10\bar{1}0)$ surfaces were re-etched.

3. Alignment of Test Fixture.

Although the loading apparatus (Figure 3) was not self-aligning, it was possible to maintain the two tungsten platens parallel to within 1×10^{-4} inch and the load axes of upper and bottom test sections coincident to 0.5×10^{-4} inch.

Each specimen was tested for loading surfaces parallel to within 1×10^{-4} inch. Crystals which did not meet this specification were not used.

4. The Creep Test.

Tests were conducted in a purified nitrogen atmosphere. The test specimen was placed in the furnace between alignment lines on the lower platen, whereupon it was heated to test temperature at the rate of about 2.5°C per minute. The specimen was held at the test temperature for one hour before application of the load. The upper loading fixture was then lowered to the specimen surface, whilst the operation was viewed through a 10X magnifying glass placed in a furnace viewing port. Following the creep test, the specimen was cooled at the rate of about 2.5°C per minute to room temperature.

Chapter III

EXPERIMENTAL RESULTS

a) Etch Pit Densities before Test and Distribution of Forest Dislocations

The results of a study of eight test specimens are reported here. Average etch pit counts of each specimen on both $(10\bar{1}0)$ surfaces before the creep test, and basal plane after the test are tabulated in Table I.

TABLE I

Average Etch Pit Counts on $(10\bar{1}0)$ Surfaces Before Test and on (0001) Basal Plane After Test.

Specimen	Average Dislocation Density on $(10\bar{1}0)$ Surfaces Before Test $(cm^{-2}) \times 10^5$	Average Dislocation Density on (0001) Surfaces After Test $(cm)^{-2}$
1C-3	2.6	$5.4 \pm 0.5 \times 10^4$
2C-3	1.9	$1.0 \pm 0.4 \times 10^5$
2C-4	4.5	$1.1 \pm 0.3 \times 10^5$
3C-2	2.5	$1.8 \pm 0.6 \times 10^5$
3C-3	1.5	$2.3 \pm 0.7 \times 10^5$
3C-4	1.5	$1.8 \pm 0.6 \times 10^5$
4C-3	1.7	$1.6 \pm 0.6 \times 10^5$
4C-4	1.6	$1.4 \pm 0.5 \times 10^5$

The dislocation etch pits on $(10\bar{1}0)$ planes were quite uniformly distributed over the surface (see Figures 6, 7, 8).

Substructure consisted of low-angle tilt boundaries perpendicular to the basal plane. These were spaced, on the average, about 0.02 inch apart and often were more than 0.2 inch in height. The low-angle boundaries could not generally be traced from one $(10\bar{1}0)$ surface to the opposite face of a test specimen. However, the density of random dislocations was always similar on both $(10\bar{1}0)$ faces.

Dislocation patterns on the (0001) basal plane, however, were not reproducible from specimen to specimen. Etch pit densities on the basal surfaces, exposed after creep testing, varied. Large clusters of non-basal forest dislocations were observed separated by areas of relatively low density (Figure 9b). Etch pit densities varied by up to 100 per cent over different areas of one specimen.

b) Decrease in Resolved Shear Stress in Constant Load Tests

The creep tests were carried out under constant load and as each test specimen was compressed, the resolved shear stress on the basal plane decreased. The resolved shear stress and shear strain were then calculated from the applied load and deflection by the relations given by Bowen and Christian (1965) for the case of compression in single slip:

$$\gamma(t) = \frac{\left\{(l_o/l(t))^2 - \sin^2\theta_o\right\}^{1/2} - \cos\theta_o}{\cos\lambda_o}$$

$$\sigma(t) = \frac{L}{A_o}\left(\frac{l(t)}{l_o}\right)^2 \cos\lambda_o \left\{1 - \left(\frac{l(t)}{l_o}\right)^2 \sin\theta_o\right\}^{1/2} \qquad (1)$$

where

$\sigma(t)$ = resolved shear stress on basal plane at time, t

$\gamma(t)$ = resolved shear strain on basal plane at time, t

l_o = initial length of specimen

$l(t)$ = length of specimen at time, t

L = applied load

A_o = initial cross-sectional area of test specimen

θ_o = initial angle between load axis and normal to glide plane

λ_o = initial angle between load axis and slip direction

The initial and final values of resolved shear stress are given in Table II. It may be noted from the Table, that the decrease in stress for all tests was less than 1.4 per cent.

TABLE II

Summary of Initial and Final Test Conditions for the Eight Test Specimens

Specimen	Initial Resolved Shear Stress (psi)	Final Resolved Shear Stress (psi)	Percent Decrease in Resolved Shear Stress (per cent)	Instantaneous Plastic Strain $\frac{in}{in} \times 10^3$	Final Strain $\frac{in}{in} \times 10^3$	Test Duration (min)	Test Temperature (^oC)
1C-3	15.66	15.63	0.19	0.7 ± 0.1	2.47	101	150
2C-3	22.54	22.42	0.54	3.0 ± 0.2	7.63	41	150
2C-4	29.91	29.67	0.81	4.8 ± 0.2	11.78	69	100
3C-2	28.30	28.17	0.46	1.2 ± 0.2	7.17	135	150
3C-3	37.43	37.33	0.27	0.2 ± 0.1	4.33	35	150
3C-4	39.88	39.57	0.78	6.8 ± 0.2	11.00	40	150
4C-3	29.97	29.81	0.54	2.8 ± 0.2	7.97	26	150
4C-4	34.93	34.47	1.33	7.4 ± 0.2	19.92	83	140

c) The Creep Experiment

1. General Nature of the Creep Curve.

Curves of basal resolved shear strain versus time obtained for the eight test specimens are plotted in Figures 10 to 14. These creep curves show all the same general form; e.g. instantaneous plastic strain followed by a decreasing creep rate referred to as the primary stage. After a period of the primary creep, the creep rate in two cases (1C-3 and 3C-3) decreased abruptly: to zero. Finally, the strain increased and the creep continued.

This final stage is referred to as terminal creep. The creep test for specimen 3C-3 was terminated in the region between the primary and terminal creep stage.

2. Dislocation Configuration after Creep.

Six distinct features become evident from the photomicrographs of Figures 15 to 19, taken after the creep test:

(i) An increase in random dislocation density from the unstrained state.

(ii) Large pile-ups of dislocations at low-angle tilt boundaries.

(iii) Areas of negligible dislocation density between some low-angle boundaries.

(iv) "Active" slip planes, or single planes of basal dislocations, which always extended to at least one specimen edge, but often propagated across the $(10\bar{1}0)$ plane from a loading surface to a free surface.

(v) Polygonization of the random dislocations.

(vi) An increase in the number of active slip planes with applied stress.

It appeared that the low-angle boundaries were effective barriers to dislocation motion. An experiment was conducted in which a tested specimen was cleaved on the basal plane at a point which bisected a low-angle boundary. The (0001) basal plane was etched and a large cluster of non-basal forest dislocations was revealed near the $(10\bar{1}0)$ plane, at the point of the sub-boundary (see Figure 20).

Pile-ups at individual low-angle boundaries did not in general extend the distance between adjacent boundaries. The fact that pile-ups consisted of both dislocations in the active slip planes and the random matrix, indicated that slip was not concentrated in the active planes only, but rather that dislocations were mobile both in the active planes and matrix.

In each specimen several areas similar to that shown in Figure (18b) were observed. In these areas of low dislocation density, traces of the active planes were often non-existent, although the same slip plane appeared active on both sides of these low density regions.

An attempt was made to trace the active slip planes from one $(10\bar{1}0)$ surface to another. Thus a tested specimen was cleaved into two sections along the basal plane, and the $(10\bar{1}0)$ planes of both sections were etched. It appeared that, in each section, some active slip planes extended across the specimen.

Specimen 3C-3 was strained only to the end of the primary creep region. Its photomicrographs then revealed that about 10 per cent of the visible active slip planes had not propagated to a considerable length in the $\langle\bar{1}2\bar{1}0\rangle$ direction on the $(10\bar{1}0)$ surface.

d) Dislocation Density Changes

The results of dislocation density measurements are summarized in Table III.

TABLE III

Summary of Average Etch Pit Counts on $(10\bar{1}0)$ Planes

Specimen	Dislocation Density on $(10\bar{1}0)$ Planes		Change in Dislocation Density	Final Resolved Shear Strain
	Before Test	After Test		
	$(cm^{-2}) \times 10^{-5}$	$(cm^{-2}) \times 10^{-6}$	$(cm^{-2}) \times 10^{-6}$	$\frac{in}{in} \times 10^{3}$
1C-3	2.6	1.6 ± 0.2	1.3 ± 0.3	2.47
2C-3	1.9	2.2 ± 0.2	2.0 ± 0.2	7.63
2C-4	4.5	2.9 ± 0.2	2.4 ± 0.3	11.78
3C-2	2.5	2.4 ± 0.2	2.1 ± 0.3	7.17
3C-3	1.5	1.8 ± 0.2	1.6 ± 0.3	4.33
3C-4	1.5	2.5 ± 0.1	2.3 ± 0.2	11.00
4C-3	1.7	2.3 ± 0.2	2.1 ± 0.3	7.97
4C-4	1.6	2.9 ± 0.1	2.7 ± 0.2	19.92

The change in dislocation density on $(10\bar{1}0)$ planes versus final resolved shear strain is plotted in Figure 21. Measurements of Adams et al (1965a) of strain-rate tests for basal slip in 99.999 per cent pure zinc at room temperature are included for comparison on the same graph. It should be noted that the crystallographic orientation with respect to the load axis of the test specimens employed here was the same as that used by Adams et al.

A curve of the form

$$\Delta\rho = C\gamma^n \qquad (2)$$

where

$\Delta\rho$ = dislocation density change, cm^{-2}

γ = resolved shear strain, in/in.

n = 0.39

C = 1.37×10^7

could be fitted to the test points for the specimens tested at 150°C. Specimens 2C-3, 3C-2 and 4C-3 were strained to approximately the same final strain, but with widely different resolved shear stresses (Table II). It is noticed that within experimental error the changes in dislocation densities were equal.

e) Stress Dependence of the Number of "Active" Slip Planes

The results of measurements of the number of active slip planes at various resolved shear stresses are summarized in Table IV.

TABLE IV

Dependence of the Number of Active Slip Planes on Applied Resolved Shear Stress.

Specimen	Number of Active Slip Planes per Inch in $\langle 0001 \rangle$ Direction x 10^{-2}	Applied Resolved Shear Stress (psi).
1C-2*	15 ± 1	23.12
1C-3	7 ± 1	15.66
2C-1	14 ± 1	22.54
2C-2	21 ± 1	29.91
3C-2	21 ± 3	28.30
3C-3	22 ± 2	37.43
3C-4	31 ± 2	39.88
3C-5	20 ± 2	29.97
3C-6	25 ± 2	34.93

* 1C-2 strained to $3.01 \times 10^{-3} \frac{(in)}{(in)}$ strain.

The measurements shown in Table IV are also plotted in Figure 22. The obtained data points can be fitted by a straight line to give a relation of the form

$$N = I\sigma - K \qquad (3)$$

where

N = number of active slip planes per inch in $\langle 0001 \rangle$ direction

σ = applied resolved shear stress

I = constant $\simeq$ 0.94

K = constant $\simeq$ 7.25

One data point, however, for the specimen 3C-3 did not fall near the experimental curve. This can be attributed to the fact that all of the active slip planes had not sufficiently expanded across the crystal and therefore the photomicrographs failed to reveal all of them.

The number of active slip planes for a given applied resolved shear stress is seen from Figure (22) to be independent of temperature. The data points of specimens 2C-4 and 4C-4 which were tested at 100°C and 140°C respectively fell on the same straight line as the points for the 150°C tests.

In addition, the N versus σ relation appeared to be independent of the resolved shear strain. Specimens 1C-2, 2C-3 deformed under approximately the same load, but the final resolved shear strains were 3.01×10^{-3} and 7.17×10^{-3} respectively. Data points for both specimens fell on the experimental curve. A similar interpretation is suggested for specimens 2C-4 and 4C-3.

f) Dislocation Relaxation

The extent of dislocation relaxation during the period between test termination and subsequent etching was not determined. However, one tested specimen was re-etched two days after the creep test. No change in dislocation configuration was seen. Thus the dislocation relaxation appeared to be negligible once the tested specimen was at room temperature.

Chapter IV

DISCUSSION

a) Validity of the Etch Pit Technique for Characterizing Plastic Deformation

Since 1956, many studies have been made of the increase in the dislocation density with plastic deformation of different ~~crystalline~~ crystalline solids. Experiments have been carried out on single and polycrystalline materials using x-ray diffraction, transmission and replica electron-microscopy, and etch pit techniques. Frequently it was found that the average dislocation density increased in form of:

$$\rho - \rho_0 = C \varepsilon^n \qquad (4)$$

where

C = constant

n = constant

ρ_0 = grown-in dislocation density, cm^{-2}

ρ = dislocation density at strain

ε = longitudinal strain, in/in.

Reid et al (1965), in a summary of the differences in the constant C for all known experiments on polycrystals and single crystals oriented for multiple slip, found that the values of C generally lay between 0.5 and 2.0 and did not appear to be sensitive to strain rate or temperature. However,

they stated that the magnitude of C depended on the grain size of the polycrystalline materials and was decreasing with increasing grain size. This implied that individual dislocations could move greater distances through the lattice at larger grain sizes.

Reid et al found a correlation between ρ_o and the value of $d\rho/d\varepsilon$ in the early stages of deformation, (5 per cent longitudinal strain for all the cases studied). Hence from the experimental data they concluded that:

$$\frac{d\rho}{d\varepsilon} = C' = K\sqrt{\rho_o}$$

where

$C' = d\rho/d\varepsilon$, cm^{-2} x per $cent^{-1}$ = value averaged over 5 per cent longitudinal strain.

K = constant

Using the value of $n = 1$, they found that:

$$\bar{d} = \frac{1}{50b\alpha K} \times \frac{1}{\sqrt{\rho_o}} \qquad (5)$$

where

$\bar{d}$ = average distance moved by dislocations

b = Burgers vector of mobile dislocations

α = fraction of the dislocations generated by deformation that were mobile.

In the case of $n = 2$, :

$$\bar{d} = \frac{1}{25b\alpha K} \times \frac{1}{\sqrt{\rho_o}} \qquad (6)$$

These relations implied that the average distance moved by the mobile dislocations was proportional to $1/\sqrt{\rho}$.

In the present results it was found that the change in dislocation density for a given strain exceeded that reported by Adams et al (1965a) by a considerable amount for strains of the order of 0.1 to 2.0 per cent (Figure 21). As the crystals used in the present experiment and those used by Adams et al were similarly prepared and had identical crystallographic orientations with respect to the compression load axis, it was felt that the marked difference in results could be attributed to one or more of the following causes:

(i) The present results were creep tests while the tests of Adams et al were strain rate tests with considerably faster strain rates ($\sim$0.001 in/in/minute) and shear stresses increasing with strain.

(ii) The present tests were conducted at 150°C while those of Adams et al were at room temperature.

(iii) The density of non-basal forest dislocation of test specimens in the present experiment was considerably in excess of that of the 99.999 per cent pure specimens used by Adams et al.

(iv) The average density of etch pits on $(10\bar{1}0)$ surfaces of samples in the present tests was more than twice that of Adams et al.

Cause (i) could be eliminated for the following reasons: Specimens 2C-1, 3C-2, and 3C-5 were compressed to about the same strain but under resolved shear stresses that differed by 50 per cent and at average strain rates that varied by about a factor of 5 (from an average rate of about 0.03 per cent per minute for specimen 3C-5 to about 0.005 per cent per minute for specimen

3C-2). The final dislocation densities agreed within experimental error. In addition, Hordon (1962), performing tensile strain-rate tests on copper oriented for single slip, found that the change in dislocation density with strain was insensitive to strain rate for strain rates of 0.6×10^{-5} sec^{-1} and 1.2×10^{-4} sec^{-1}.

The effect of temperature, however, could not be estimated from the present tests, as sufficient data for creep tests in the range $23^{o}C$ to $150^{o}C$ were not obtained.

The effect of the non-basal forest dislocation could be determined by the measurements of Adams et al in Figure (21). Their central data point, representing 1 per cent strain on a specimen with a forest density of about 9×10^{4} cm^{-2}, correlated reasonably well with the two data points which represented specimens with forest densities of about 10^{4} cm^{-2}. It would seem that, for their case, the change in basal dislocation density for a given strain did not vary very strongly, if at all, with the forest density. Also, the data points of the present tests represent specimens with forest densities varying from about 6×10^{4} to 2×10^{5} cm^{-2}, but no systematic variation in basal dislocation density change with forest density, for a given strain, could be found.

The fourth possible cause for the apparent discrepancy in results is the effect of the number of grown-in dislocations in each test specimen. Livingston (1962) carried out tensile tests on copper crystals oriented for $\langle 110 \rangle$ (111) single slip, at a strain rate of 0.001 in/in per minute. The initial dislocation densities of his specimens ranged from 10^{4} to 10^{5} cm^{-2}. He found the dislocation density-strain relation not to be

single-valued, and concluded that the dislocation density in deformed copper single crystals was more closely correlated with stress than strain. Since Livingston did not specify the density of grown-in dislocations in individual samples employed in his tests, it was not possible to determine any systematic change of the $\Delta\rho$ versus γ curve for increasing values of initial dislocation densities. The fact that the density of grown-in dislocations varied by a factor of 10 in Livingston's specimens may, however, be intimately connected with the fact that he could not closely correlate $\Delta\rho$ and γ.

Levinstein and Robinson (1963) conducted incremental shear tests on silver single crystals on the $\langle\bar{1}01\rangle$ $(1\bar{1}1)$ system at room temperature. They obtained a relation between $\Delta\rho$ and γ of the form:

$$\Delta\rho = C\gamma \tag{7}$$

where

C = Constant

for 2 specimens.

The first crystal had an in-grown dislocation density of about 1×10^8 cm^{-2}, while C was approximately 9.8×10^9 for this sample. The second specimen had an initial dislocation density of about 5×10^6 cm^{-2}, while C was 2×10^8. Levinstein and Robinson concluded from observations of the dislocation arrangement after shear deformation, that in the sample having the lower initial dislocation density, the mean free path of

the dislocations was increased. This was in qualitative agreement with the results of Reid et al (1965) for slip in polycrystals and single crystals oriented for multiple slip.

To determine if a correlation between $d\rho/d\varepsilon$ and ρ_o existed for monocrystals oriented for single slip in the early stages of deformation, linear average values of $d\rho/d\varepsilon$ were plotted versus ρ_o from the etch pit measurements of Levinstein and Robinson, Adams et al (1965a) and the present author.

In addition, a value of $d\rho/d\varepsilon$ versus ρ_o was determined for the etch pit measurements made by Hordon (1962) on tensile specimens of copper oriented for single slip.

A value of $d\rho/d\varepsilon$ versus ρ_o was also plotted for the transmission electron-microscopic dislocation density measurements made by Hirsch and Lally (1965) on magnesium single crystals deformed in easy glide. It was necessary to choose linear average values of $d\rho/d\varepsilon$ for $\varepsilon \leqslant 0.5$ per cent in order to include the measurements of Hordon. These results are plotted in Figure (23).

It is seen that C' increases monotonically for single crystals deformed in single slip. The data points follow a curve of the form:

$$C' = \frac{d\rho}{d\varepsilon} = K\rho_o^n \qquad (8)$$

where

K = constant

$n \simeq 0.5$

If the relation postulated in equation (8) is indeed a "real" one for single slip in monocrystals, it would imply that the glissile dislocations themselves are responsible for the formation of new ones during easy glide. This would be in accord with the results of Johnston and Gilman (1959) who observed the formation of many new loops on the expansion of a glide dislocation loop by an applied stress.

Although it did not seem that equation (8) was temperature-dependent in the range 23° to 150°C or dependent on forest density, results from other experiments would have to be tabulated before any conclusions could be reached in this respect.

b) Correlation between Initial Dislocation Densities and the Yield Stress

Gilman (1956), conducting tensile strain-rate tests on 99.999 per cent pure zinc single crystals oriented for basal slip, demonstrated that the initial resolved shear stress was about 15 psi and changed only slightly with strain-rate and temperature in the range of 0.3×10^{-5} to 10×10^{-5} in/in per second and 182° to 407°C , respectively. In compression strain-rate tests (0.001 in/in per minute) at room temperature on 99.999 per cent pure zinc crystals oriented for basal slip, Adams et al (1965a) found the critical resolved shear stress to be about 15 psi.

This suggests that the factor determining the critical resolved shear stress in the temperature region of about 23° to 400°C is athermal.

On the basis of the above, and of the low work hardening rate determined in the tests of Adams et al ($d\sigma/d\gamma \simeq 8.7$ psi/per cent strain), it could be concluded that resolved shear stresses of the order of 20 psi

for the present creep tests would cause instantaneous ~~plastic~~ plastic strains of the order of 0.5 per cent. As can be seen in Table II, this did not occur. Adams et al (1965a) found an increase in the critical resolved shear stress for basal glide with an increased density of non-basal forest dislocations in 99.999 per cent pure zinc. They interpreted the forest effect by means of the interaction of basal and forest dislocations to produce attractive and repulsive junctions (Saada (1960)). In this model, the critical resolved shear stress increased with the square root of the forest density. Friedel (1963) showed, however, that the stress required for a glide dislocation to cut across an attractive forest was practically independent of temperature.

The present results were interpreted qualitatively in terms of junction reactions. Test specimens 2C-4, 4C-3, and 3C-2 were tested with approximately the same resolved shear stresses, but their average forest densities were about 1.1×10^5 cm^{-2}, 1.6×10^5 cm^{-2}, and 1.8×10^5 cm^{-2}, respectively (Tables I and II).

From Table II, it is seen that specimen 2C-4, with the smallest forest density, had the greatest instantaneous plastic strain, while specimen 2C-3, with the largest forest density, underwent the smallest instantaneous plastic deformation. Assuming, for the present, that the density of basal dislocations was not responsible for the magnitude of the yield stress, it is possible to interpret the above results. For the same applied resolved shear stress, a larger instantaneous plastic deformation implies that the yield stress is lower. Thus the results agree qualitatively with Saada's model. Similar comparisons of specimens 3C-3 and 4C-3, as well as 3C-3 and 3C-4 yield the same qualitative results.

Seeger (1957) proposed in his work-hardening model that the critical resolved shear stress of a crystal oriented for easy glide was determined by the interaction of the stress fields of parallel glide dislocations. The yield or critical stress was that stress which permitted glide dislocations to overcome the opposing action of the stress fields of their parallel neighbours. He determined that the yield stress was proportional to the square root of the density of the grown-in glide dislocations.

In the present tests, no correlation could be found between the density of grown-in basal dislocations and initial plastic strain. In fact, specimen 2C-4 had an initial basal dislocation density almost $\frac{3}{4}$ times greater than that of specimen 4C-3, but as noted above, under the same applied stresses, the instantaneous plastic strain of the former was more than $1\frac{1}{2}$ times greater than that of the latter. Therefore, it seems improbable that the interaction of basal dislocations is directly responsible for the magnitude of the yield stress in zinc.

It is difficult to understand physically a model of the yield stress based solely on interaction between glide dislocations. Although the dislocations may exert forces on each other opposing the applied stress field, Seeger's theory does not explain any collective resistance of the basal dislocations to the applied stress. The glide dislocations may be held in equilibrium with respect to one another, but the theory does not provide an explanation why the body of dislocations does not move en masse through the lattice. However, it is plausible that, for a given forest dislocation density, a larger number of basal dislocations would increase the resistance to yield.

c) Characteristics of Work Hardening

The creep curves of the 8 test specimens all exhibited the same abrupt decrease in creep rate following the initial primary stage. Cottrell and Aytekin (1950) conducted constant stress creep tests on tensile specimens of spectroscopically pure zinc crystallographically oriented for basal slip. They observed a transient stage which gradually changed to steady-state creep. Their experimental curves correlated well with Andrade's creep equation:

$$\gamma = \gamma_o + Bt^{1/3} + Kt \qquad (9)$$

where

γ = Plastic strain at time t

γ_o = Initial plastic strain

B = Constant

K = Constant

t = Time

for temperatures below 120°C.

B and K were temperature and stress-dependent and varied from crystal to crystal.

Applied shear stresses in their tests varied between 60 and 90 psi. The primary region extended for periods of time from 10^4 to 10^5 seconds, while average primary and steady-state creep rates were greater than 10^{-4} in/in per minute and 10^{-5} in/in per minute respectively. Cottrell and Aytekin observed slip bands at various stages of creep and found that they became more prominent as flow progressed. They concluded that the process of slip continued on the glide planes throughout the test.

The average strain rates observed for the primary stage of creep in the present experiments were of the same order of magnitude as those found in the initial stages of transient creep of the specimens of Cottrell and Aytekin with resolved shear stresses of about 60 psi.

Following the initial primary stage of creep in the present test specimens, the creep rate was found to be much lower than that observed by Cottrell and Aytekin.

Slifkin and Kauzmann (1952) studied the transient creep of 99.999 per cent pure zinc crystals in tension at room temperature and at average strain rates of the same order of magnitude of those in the present tests. They found a creep rate, after instantaneous plastic strain, to be of the form:

$$\gamma = a t^{-n} \tag{10}$$

where

a = constant for a specific set of test conditions

n = constant for a given test, but varies from experiment to experiment.

The resolved shear stresses used in their tests were of the same magnitude as those employed in the present experiment. Slifkin and Kauzmann found that as long as the specimen deformation occurred by transient creep, annealing after each test permitted many runs to be made on a single crystal with no apparent change in the constants of the creep equation.

This meant that the changes taking place in the crystal during transient creep were not permanent. They considered that if transient creep was caused by the movement of dislocations produced by stress-induced sources such as the Frank-Read type, then the decrease in creep rate with time would be caused by the blocking of these sources. If transient creep involved the destruction of dislocation sources, then new ones would have to be produced on each anneal and it would be difficult to account for the good reproducibility of creep curves from the same specimen. Slifkin and Kauzmann believed that the instantaneous plastic strain was the result of unimpeded operation of the dislocation sources activated by the applied stress. As deformation proceeded, the accumulation of dislocations and vacancies produced from jogs on basal dislocations would exert a back stress on the dislocation sources and cause a decrease in the rate of deformation.

The photomicrographs of the test specimens used in the present experiment revealed three marked differences between the dislocation structure of specimen 3C-3, strained only into the primary stage, and that of the other specimens:

(i) not all of the active slip planes in specimen 3C-3 were well-developed.

(ii) pile-ups at low angle boundaries consisted both of dislocations on the active planes plus large numbers of polygonized dislocations between the active planes on all specimens except 3C-3. For this crystal, pile-ups were composed of dislocations on the active planes but few pile-ups of polygonized dislocations were seen.

(iii) large areas between pile-ups that were relatively free of dislocations were found on all specimens except 3C-3.

It would be premature, on the basis of the limited results of this experiment, to draw definite conclusions as to the rate of propagation of the active slip planes across the crystal and its effect on the form of the creep curve. However, if slip in the primary stage is controlled by the speed at which these lines are formed, then the abrupt drop in the creep rate after the primary region could be explained as follows. The initial dislocations emitted by the surface sources travel considerable distances across the crystal and many escape at the opposite face. As deformation continues, new dislocations are piled up at barriers and exert back stresses on the source. Eventually the extent of the back stress is such that the surface source can emit no further dislocations, and deformation on the slip plane stops. If the barriers to dislocation motion are evenly distributed across the $(10\bar{1}0)$ surface, then deformation will stop on many of the active planes at about the same time.

Creep could continue in the specimen if dislocations in the active planes were annihilated by some thermal process, thus releasing the back stresses on the surface sources and/or if movement of dislocations in the matrix, separate from forces exerted by the dislocations in the active planes, became rate-controlling.

It was noted previously that some active planes could be traced from one prism plane to another. This implied that the grown-in dislocation loops expanded across the crystal during deformation. As the resolved shear stress in the direction of the Burgers vector parallel to the $(10\bar{1}0)$

prism planes was the greatest, most of the etch pits on the prism surfaces would be primarily of edge character. It is possible that on expansion of the active planes across the test specimen, random dislocations from the matrix become "attached" to dislocations in the active planes because of attractive interaction of their stress fields, thereby reducing the elastic energy of the lattice. This would lead to mechanical polygonization of the random dislocations. Sinha and Beck (1961) observed mechanical polygonization of basal dislocations on bending of 99.999 per cent pure zinc crystals.

The large areas of relatively low dislocation density found between sub-boundaries on specimens strained into the final stage of creep in addition to the pile-ups of both random dislocations and those in the active planes indicate that the sub-boundaries (or large clusters of non-basal dislocations which possibly are responsible for their formation during crystal growth) are strong barriers to dislocation motion and therefore are responsible for work-hardening of the crystal. This has been indicated before for zinc (Adams et al (1965a)).

d) Distribution of the Active Slip Planes

When the experimental curve of Figure 22 is extrapolated to the point where $N = 0.$, it is found that the applied stress at this point is about 7.5 psi. If the straight-line relationship is valid, no active slip planes should be formed for applied stresses below about 7.5 psi. This implies that below this level, no appreciable redistribution or increase of dislocation density would occur. Adams et al (1965b) found

that stress pulses of magnitude less than 7 psi produced no increase of dislocation density, although they observed occasional local rearrangement of dislocations. They observed pile-ups of dislocations for stress pulses of magnitude greater than 7 psi.

Basinski and Basinski (1964) observed glide bands, or regions of low dislocation density, between deformation bands in tensile testing of copper single crystals strained in stage I. The glide bands were parallel to the primary slip plane. They observed that at lower strains, the bands contained etch pits in single file. They found that the spacing between the glide bands decreased with increasing strain (or stress, as tests were of the strain-rate type). Basinski and Basinski then determined a relation between the spacing of the glide bands and the flow stress of the form:

$$N = C\sigma^{n} \tag{11}$$

where

C , n are constants

N = number of bands per cm.

σ = applied shear stress.

These bands seem similar in character to the active slip planes observed in the present tests.

It is a well-known fact that an increase or decrease in the applied stress in a creep test on single or polycrystalline materials is responsible for an acceleration or slowdown of the creep rate (Conrad (1961)).

On the basis of the data from the present results it would seem that the relation between the number of active slip planes and applied stress is temperature independent. If this is indeed the case, and if it is confirmed that the primary stage of creep is controlled by the slip in the active planes, then:

$$\left(\frac{\partial \dot{\gamma}}{\partial \sigma}\right)_T = \text{Const.} \tag{12}$$

where

$\dot{\gamma}$ = strain rate

σ = applied resolved shear stress

T = temperature.

or the change of strain rate to the applied resolved shear stress would be independent of temperature. Conrad and Robertson (1957) (1958) found that $\left(\frac{\partial \ln \dot{\gamma}}{\partial \sigma}\right)_T$ was temperature-independent in the range of 78° to 364°C for creep of magnesium single crystals in tension. Conrad et al (1961) explained this in terms of a modification to Seeger's dislocation-intersection model.

Cottrell and Aytekin (1950) found that:

$$\left(\frac{\partial \ln \dot{\gamma}}{\partial \sigma}\right)_T$$

was independent of temperature in the range 23° to 128°C for creep of zinc single crystals in tension.

Adams et al (1965a) have proposed that the mechanism for basal slip in zinc at room temperature is not thermally activated. A model for the deformation based partially on the fact that the number of active slip planes (or sources) increases with applied stress could explain the stress-dependence of the creep rate in terms of the mobile dislocations made available through sources activated by a stress increase.

Chapter V.

SUMMARY AND CONCLUSIONS

Changes in basal direction density during compression creep tests of 99.999 per cent pure zinc single crystals have been experimentally measured. The change in density could be approximated by :

$$\Delta\rho = C\,\gamma^{0.39}$$

This relation appeared to be independent of the resolved shear stress during creep and the average creep rate. The value of the constant C was found to be extremely sensitive to the density of grown-in basal dislocations of the test specimens. The temperature-dependence of the empirical equation was not determined.

An abrupt decrease in the creep rate after an initial primary stage was observed for all tested specimens. However, sufficient data was not available to reliably report its cause.

The critical resolved shear stress of the test specimens was shown qualitatively to depend on the density of forest dislocations.

The number of active slip planes, or single rows of dislocations that stretched across the prism surfaces, was found to be directly proportional to the applied stress, satisfying the experimental equation:

$$N = I\sigma - K$$

This relation was independent of strain and temperature in the range 100° to 150°. The stress below which no active planes should appear was in quantitative agreement with previous results obtained by pulse-loading of pure zinc crystals. The fact that the number of active slip planes was strongly dependent on the applied stress was offered as a possible explanation of the change in creep rate associated with a variation in applied stress for deformation processes not thermally activated.

The appearance of large areas of low dislocation densities between pile-ups at sub-boundaries in specimens strained to the final stage of creep suggested a work-hardening model for deformation of zinc on the basal system based on the internal stress fields associated with these pile-ups.

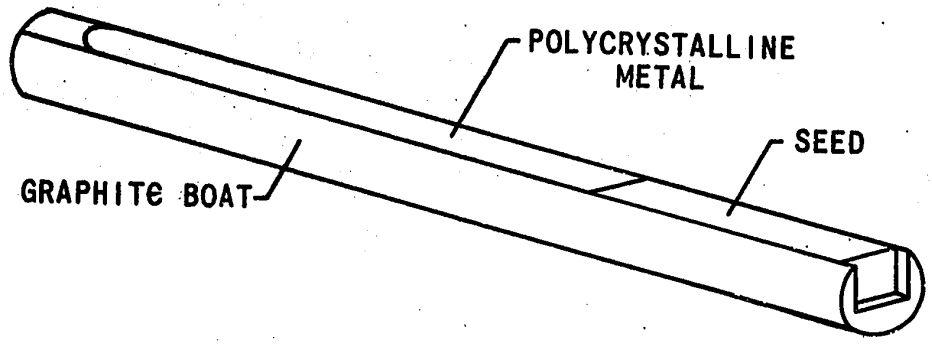

SCALE: 1/2"= 1"

(A) ARRANGEMENT FOR CRYSTAL PREPARATION FROM A SEED

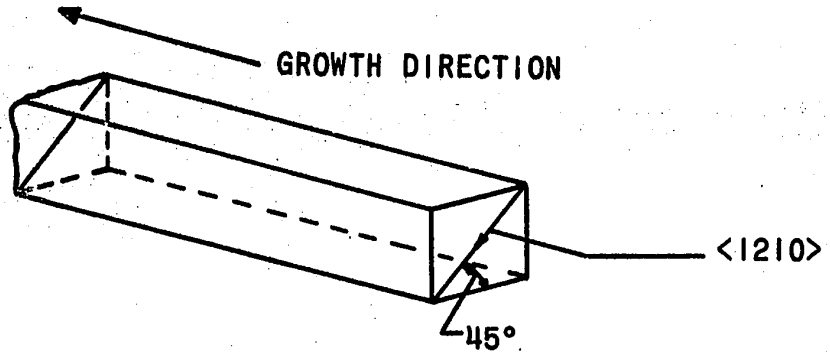

SCALE: APPROX.FULL SIZE

(B) CRYSTAL ORIENTATION WITH RESPECT TO GROWTH DIRECTION

FIG. 1

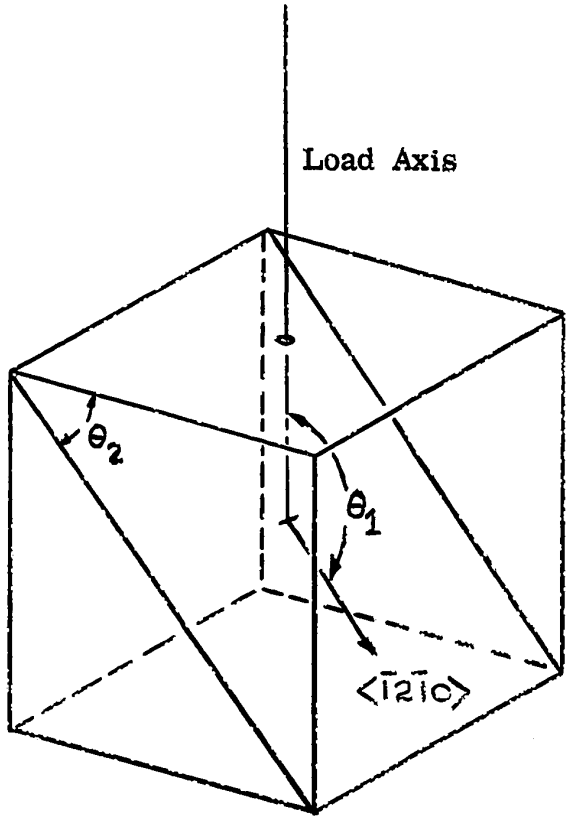

(0001) Basal Plane

$(10\bar{1}0)$ Prism Plane

Uncertainty in Crystallographic Orientation

Angle	Nominal Value	Uncertainty
θ_1	135^o	$\pm 1^o$
θ_2	0^o	$\pm 1^o$

Figure 2.

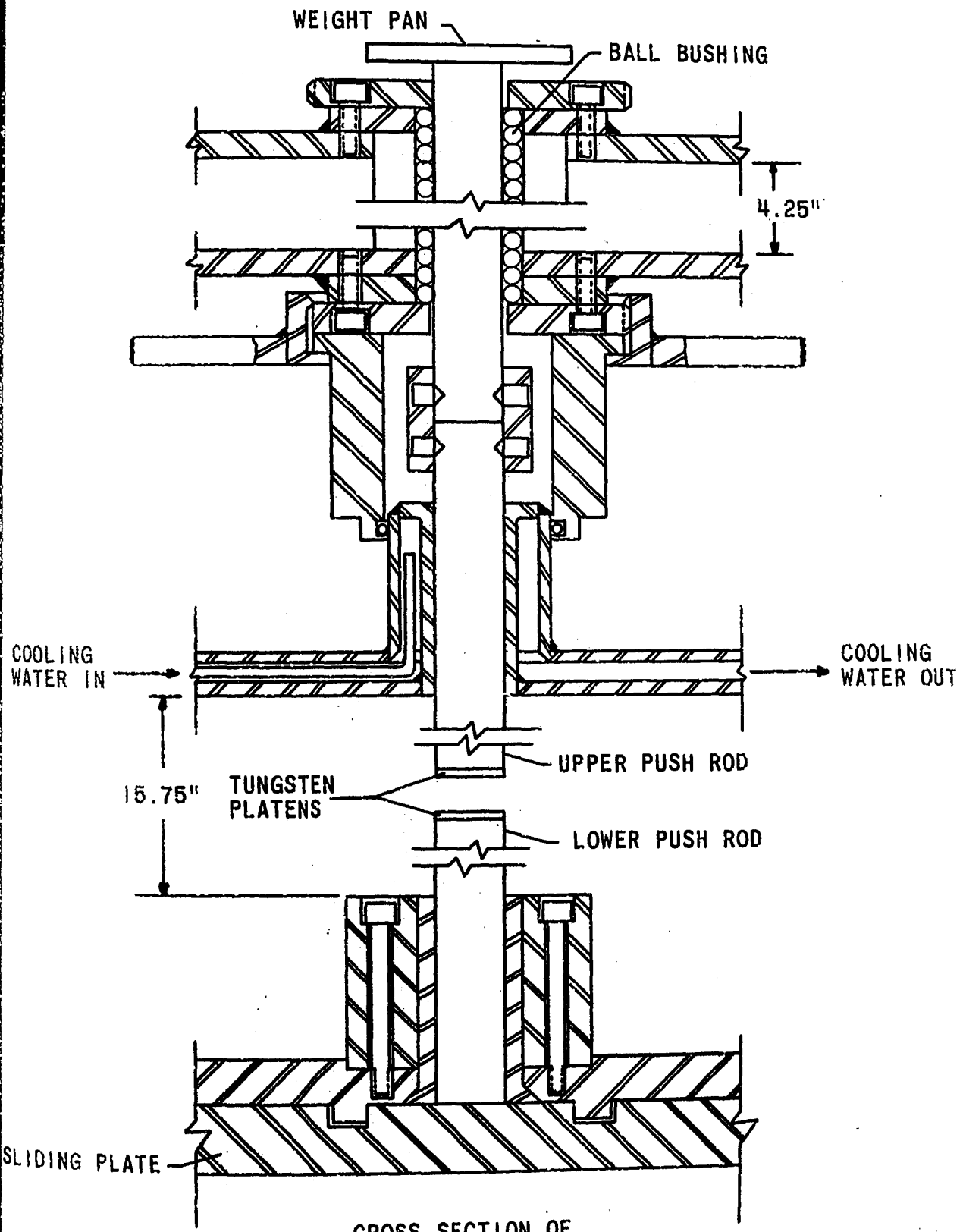

CROSS-SECTION OF LOADING APPARATUS

SCALE: 1/2" = 1"

FIG.3

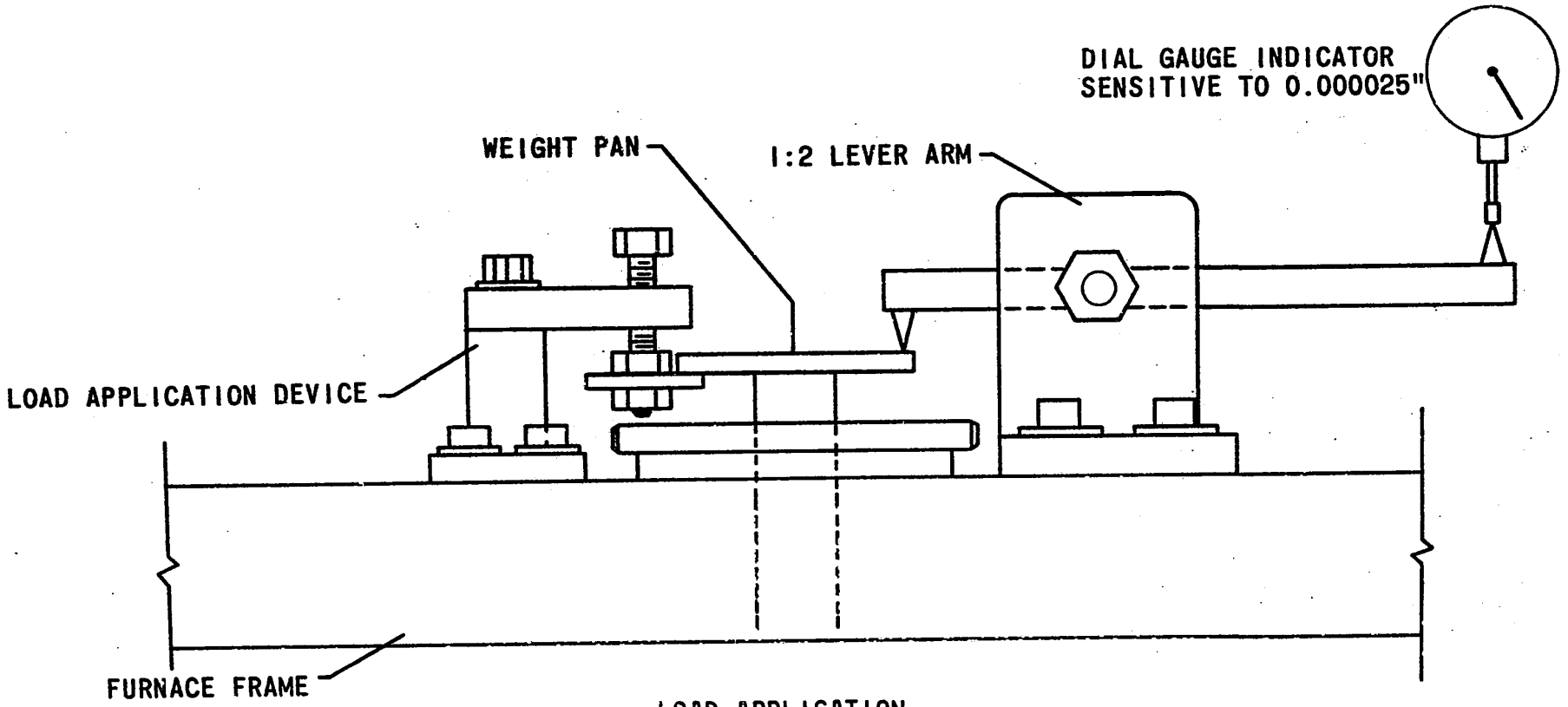

LOAD APPLICATION
AND
STRAIN-MEASURING APPARATUS

SCALE: 1/2" = 1"

FIG. 4

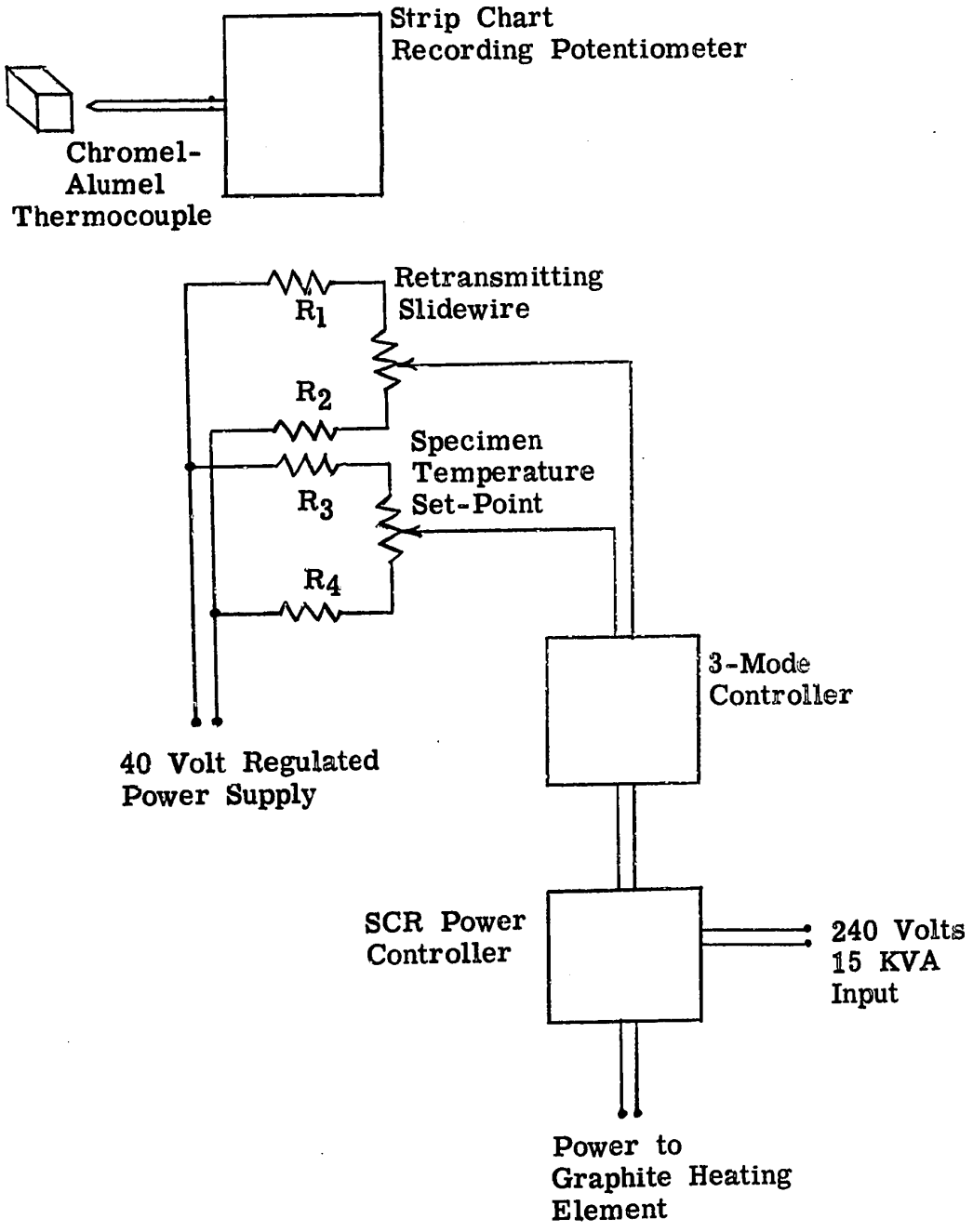

Temperature Control Circuit

Figure 5.

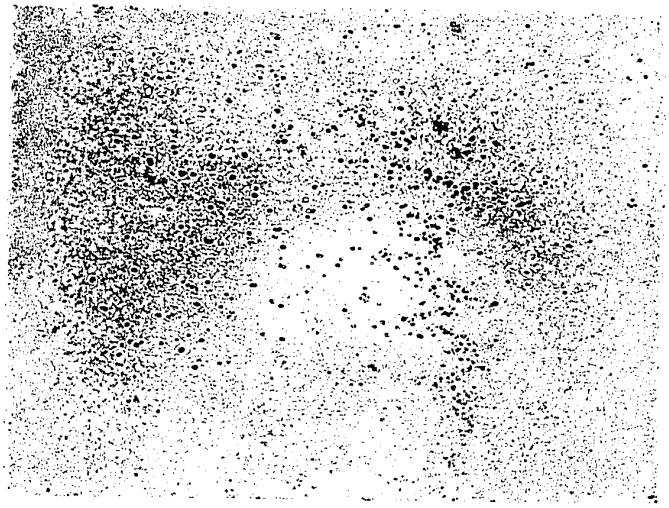

(a) Specimen 1C-3 112.5X

$(10\bar{1}0)$
—— $<\bar{1}2\bar{1}0>$

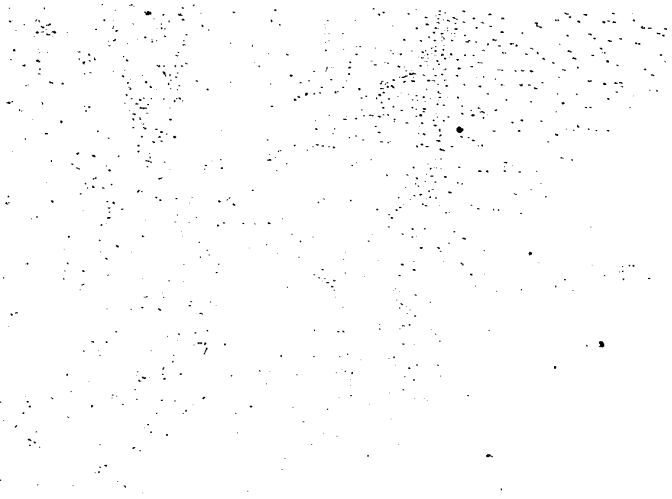

(b) Specimen 2C-3 100X

Typical Areas on the $(10\bar{1}0)$ Prism Planes of Annealed, Untested Specimens Dislocations Revealed as Etch Pits

Figure 6.

Low-angle Tilt Boundary

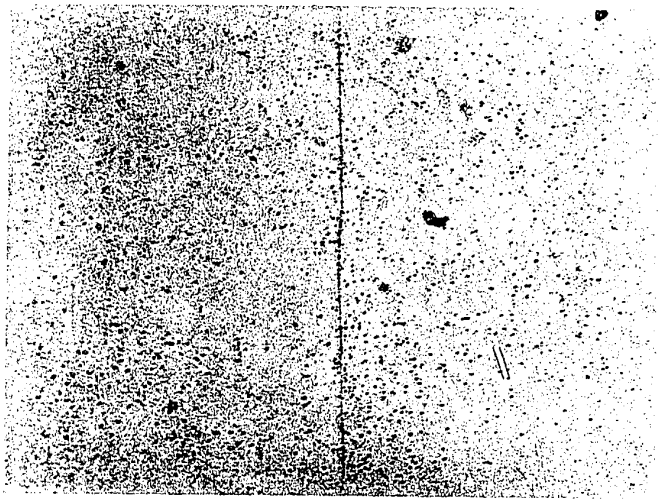

(a) Specimen 3C-2 100X

$(1\bar{0}10)$
—— $<\bar{1}2\bar{1}0>$

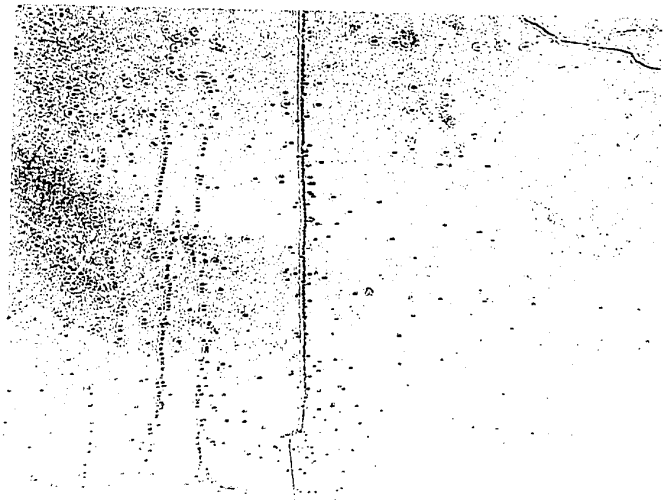

(b) Specimen 3C-3 100X

Typical Areas on the $(1\bar{0}10)$ Prism Planes of Annealed, Untested Specimens.

Figure 7.

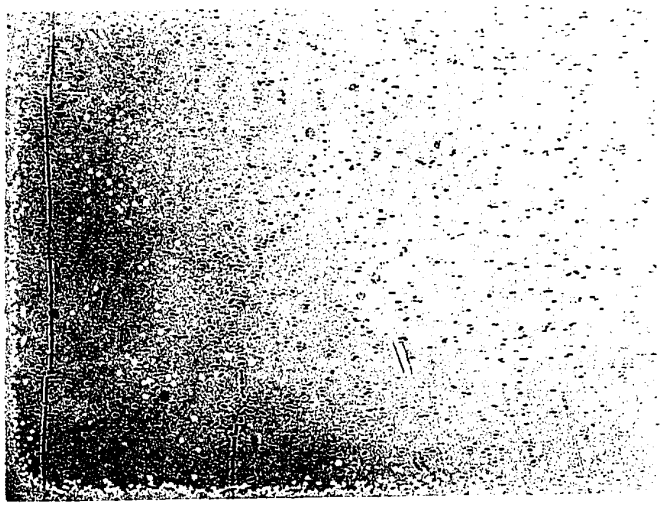

(a) Specimen 4C-3 100X $\frac{(10\bar{1}0)}{<\bar{1}2\bar{1}0>}$

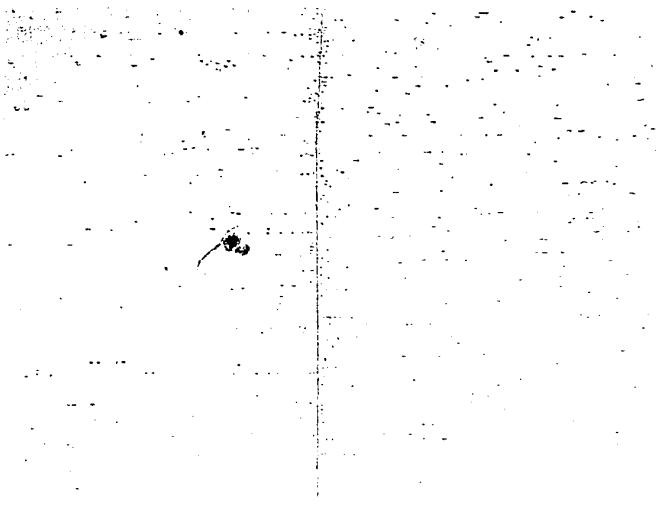

(b) Specimen 4C-4 100X

Typical Areas on the $(10\bar{1}0)$ Prism Planes of Annealed, Untested Specimens.

Figure 8.

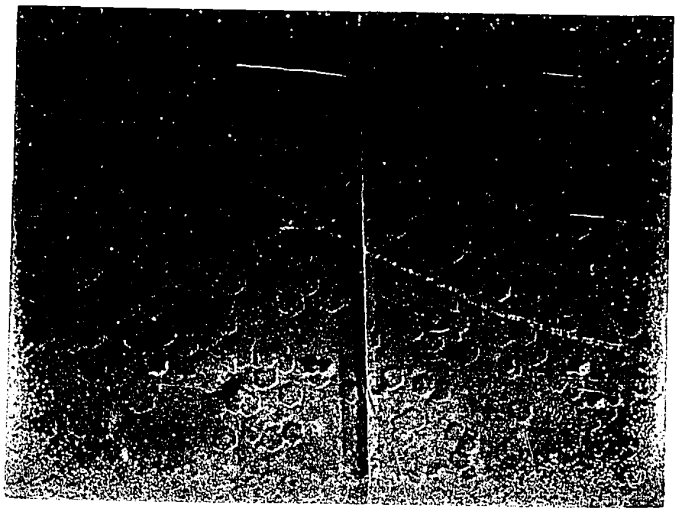

(a) Specimen 1C-3 100X

(0001)
$\langle \bar{1}2\bar{1}0 \rangle$

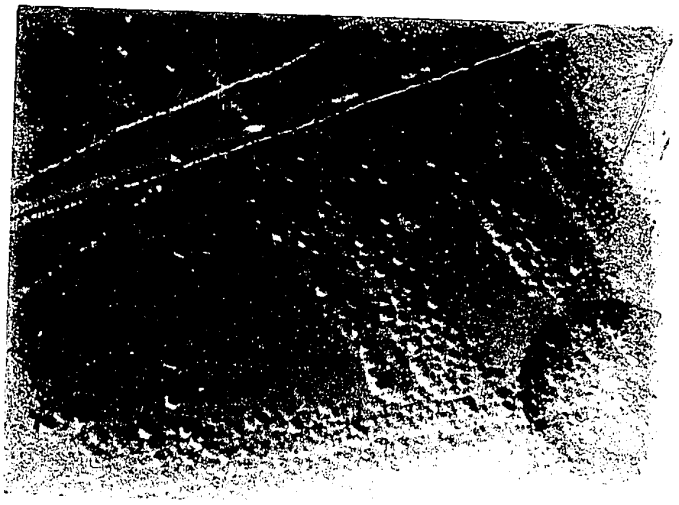

(b) Specimen 3C-2 75X

Non-Basal Dislocations Exposed as Hexagonal Etch Pits on the Basal Plane. After Testing. Oblique Illumination.

Figure 9.

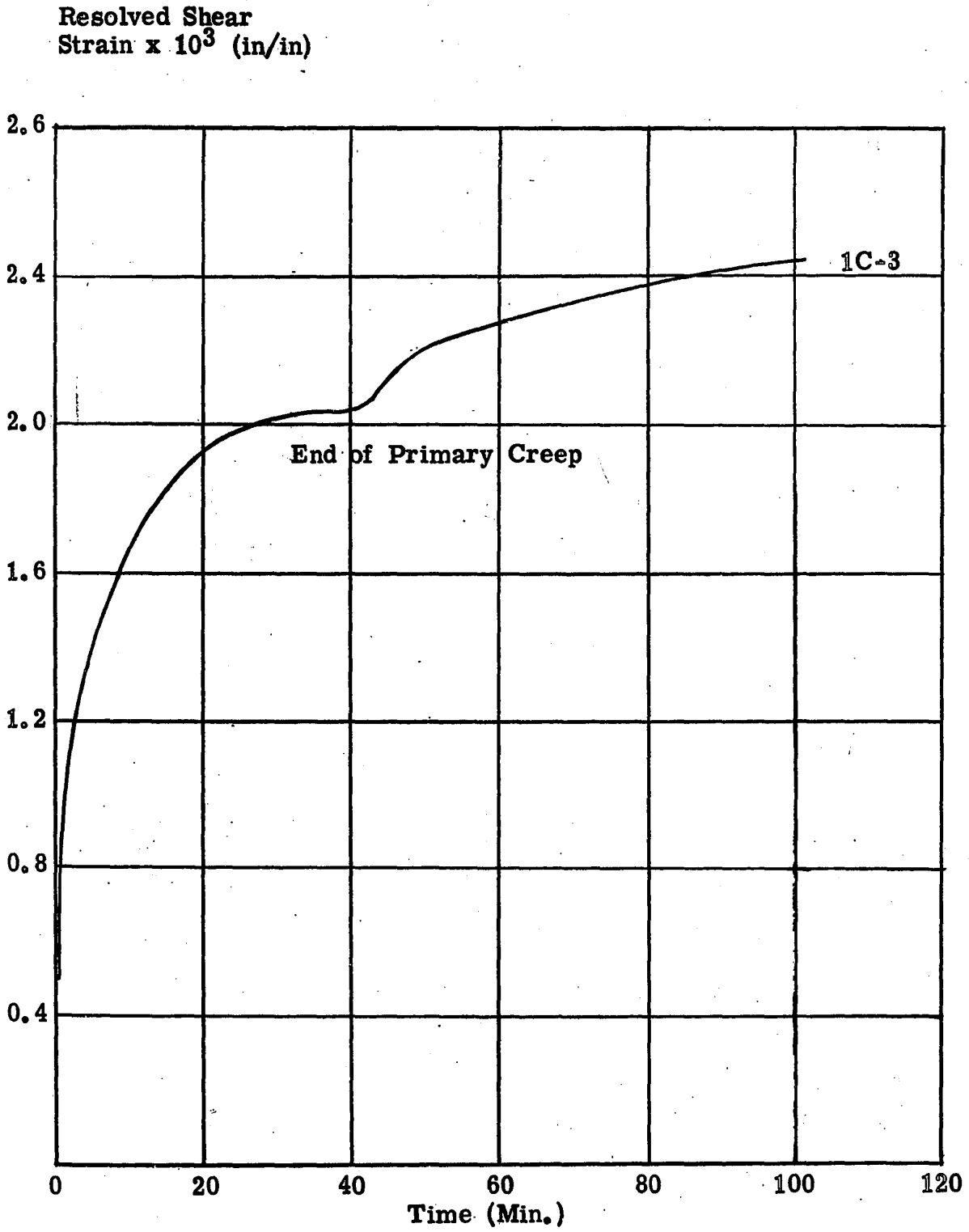

Creep Curve for Basal Slip of Specimen 1C-3

Figure 10.

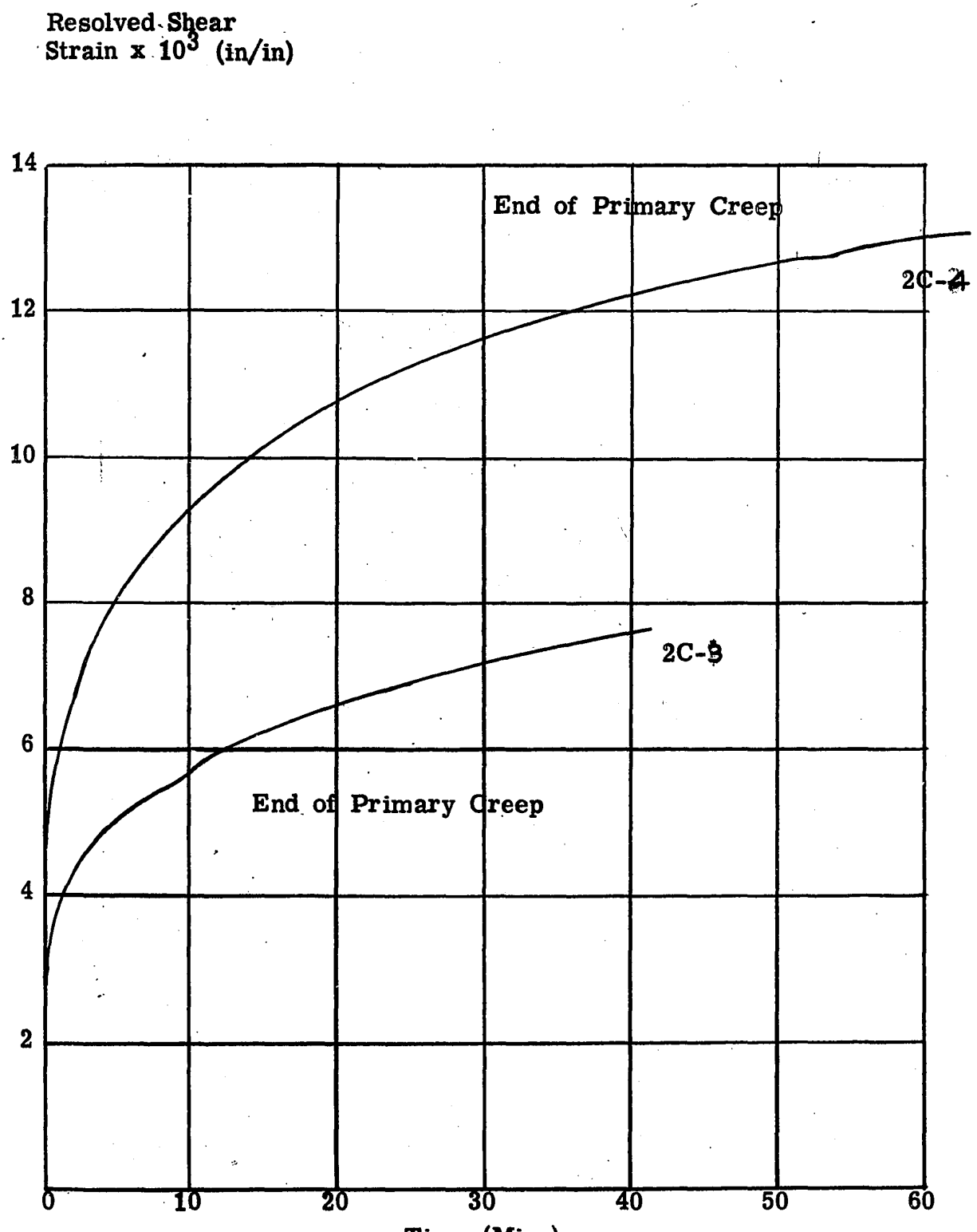

Creep Curves for Basal Slip of Specimens 2C-3 and 2C-4

Figure 11.

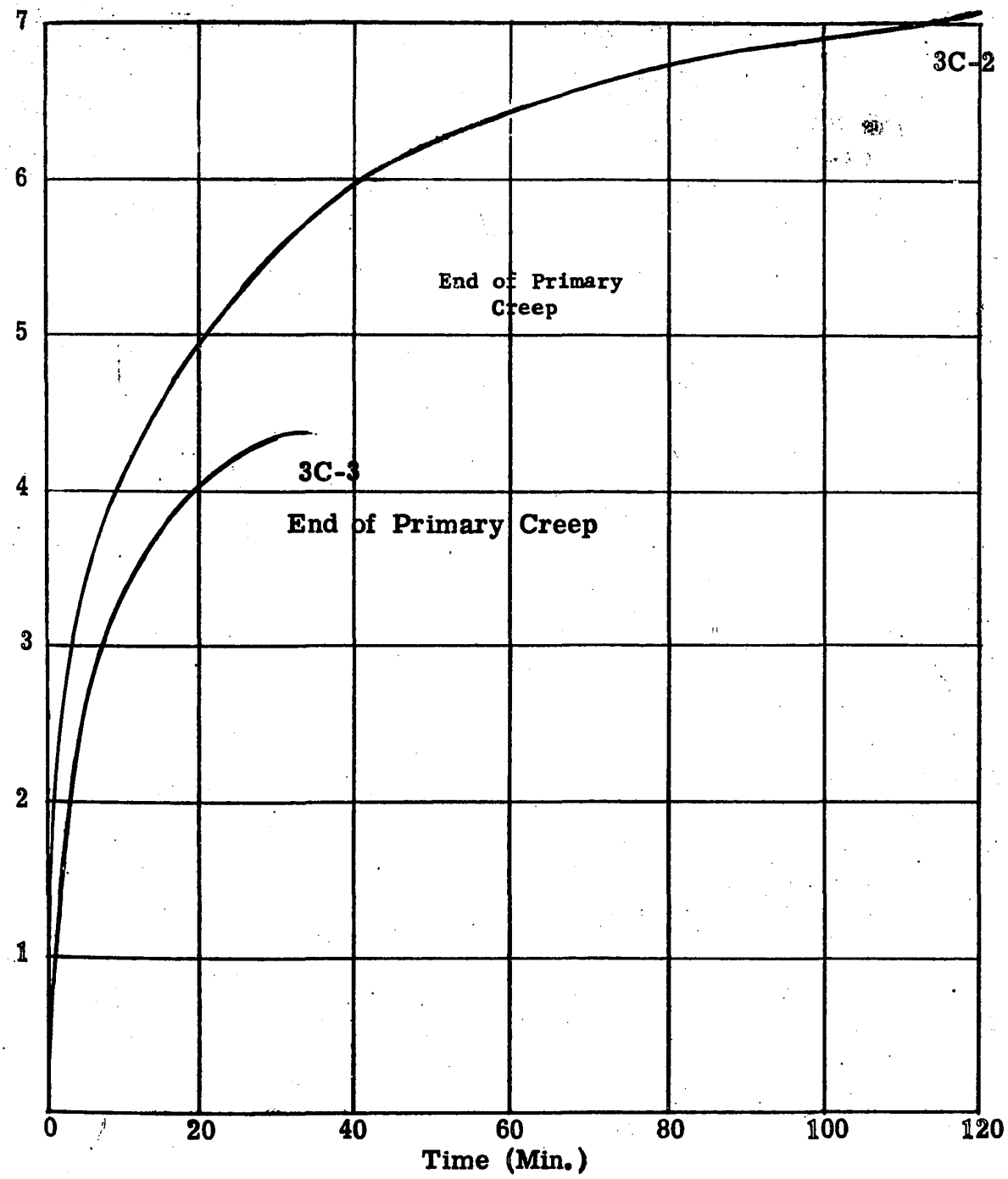

Creep Curves for Basal Slip of Specimens 3C-2 and 3C-3

Figure 12.

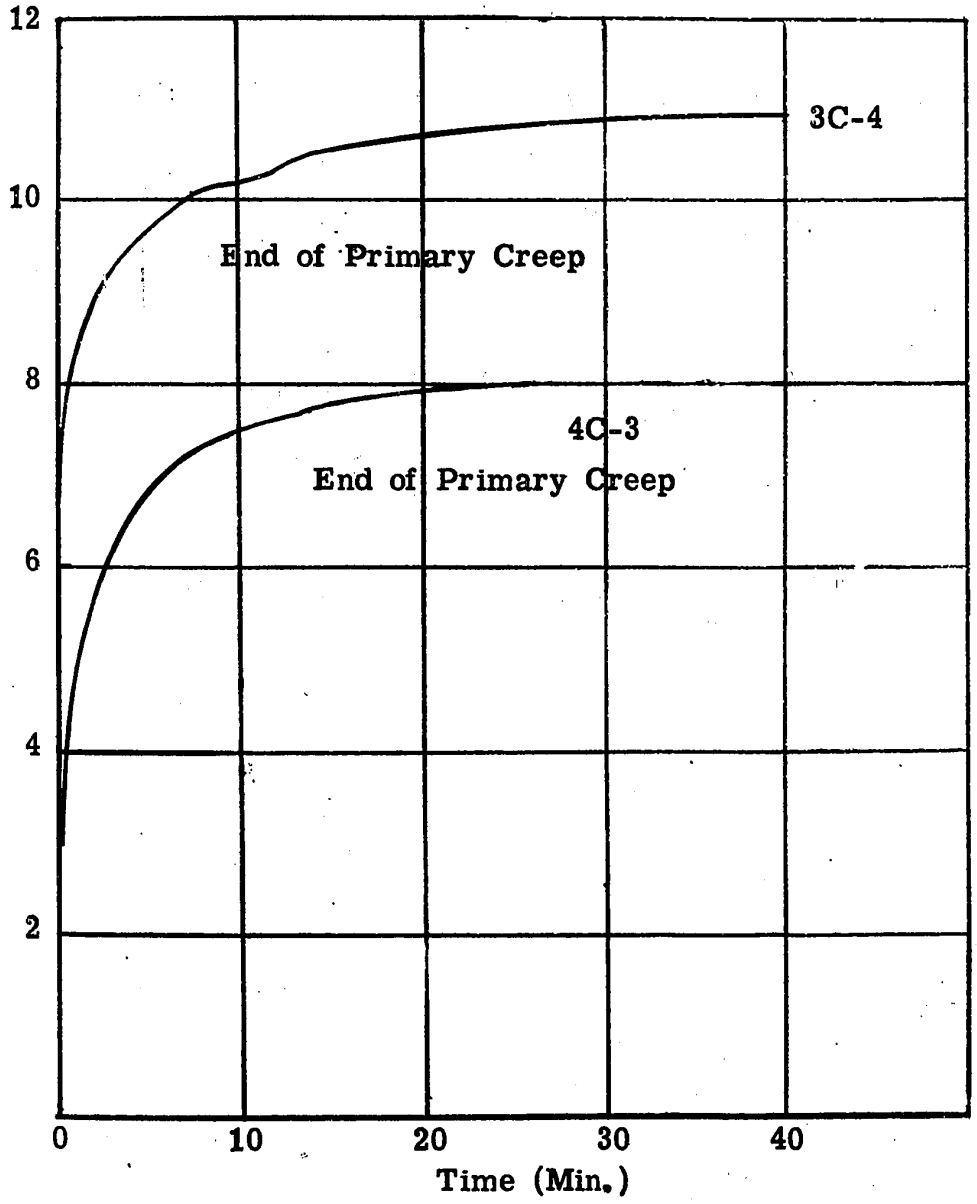

Creep Curves for Basal Slip of Specimens 3C-4 and 4C-3

Figure 13.

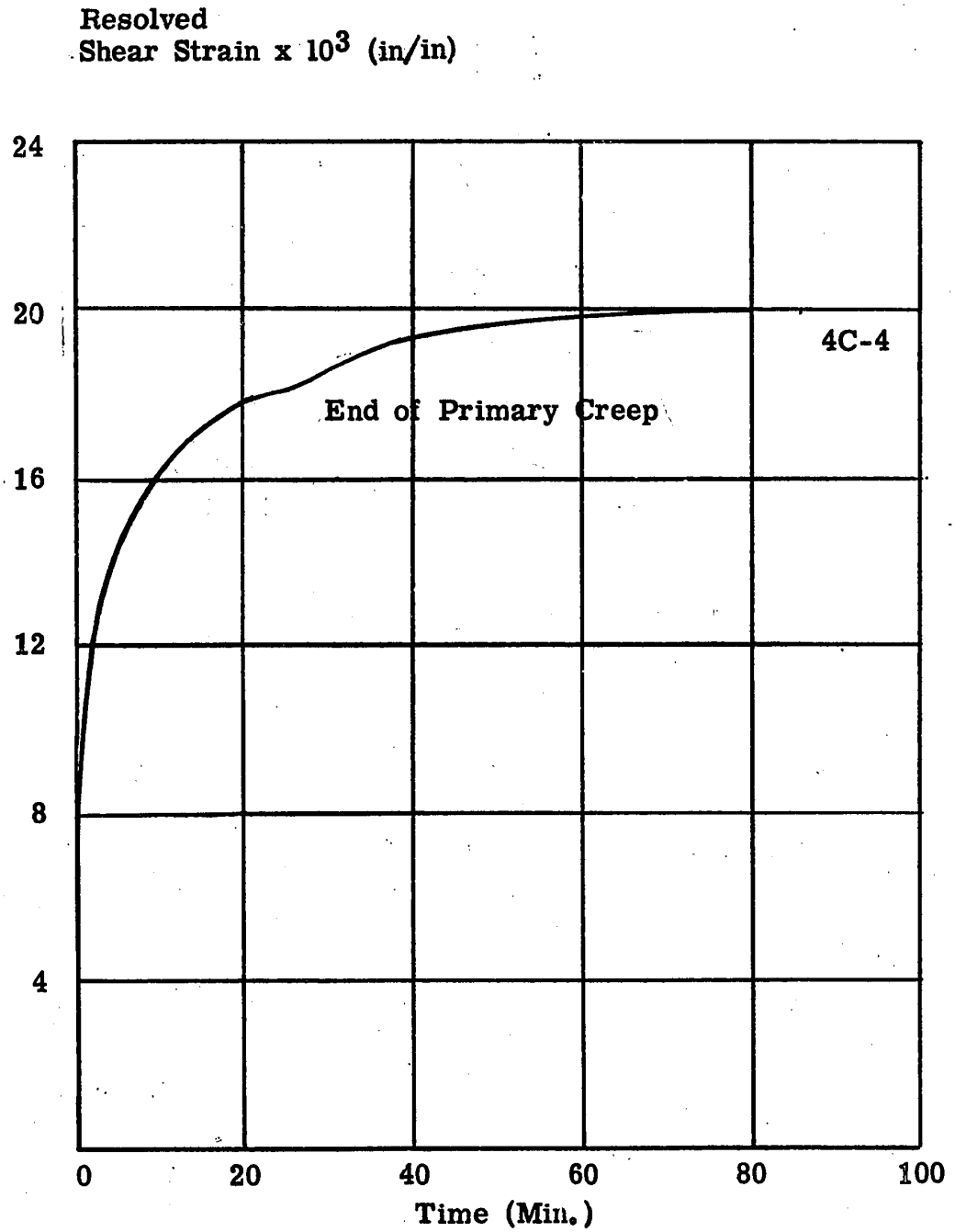

Creep Curve for Basal Slip of Specimen 4C-4
Figure 14.

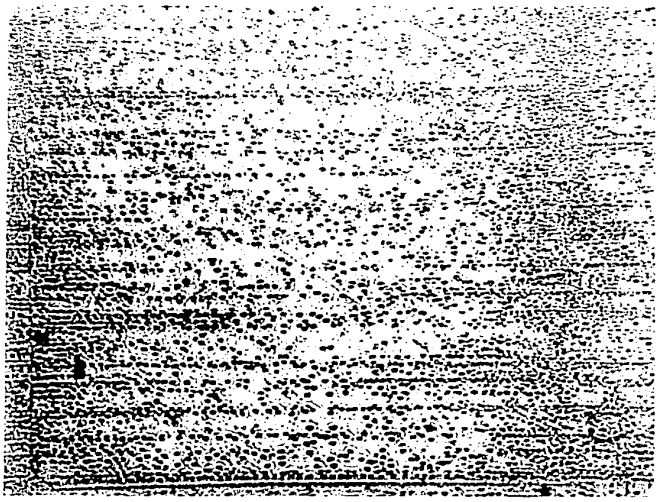

(a) Specimen 1C-3 150X

$(10\bar{1}0)$
—— $<\bar{1}2\bar{1}0>$

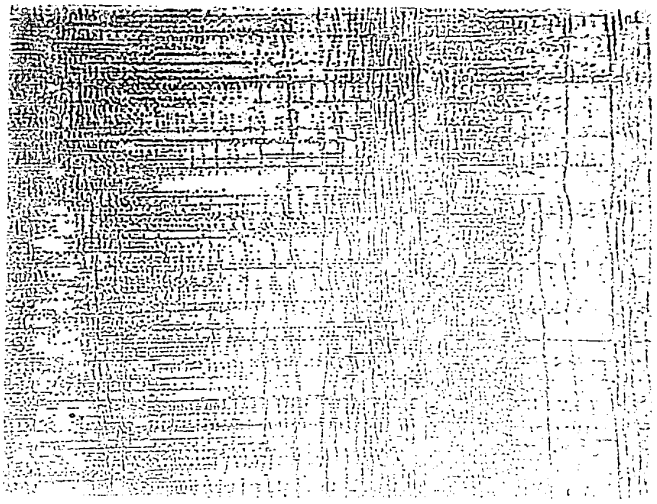

(b) Specimen 2C-4 150X

Areas on the $(10\bar{1}0)$ Prism Planes of Specimens After Creep Testing

Figure 15.

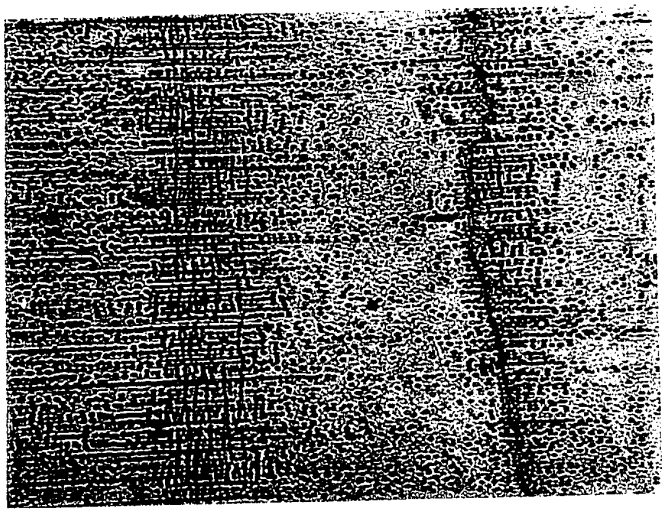

(a) Specimen 3C-2 150X

$(10\bar{1}0)$
—— $<\bar{1}2\bar{1}0>$

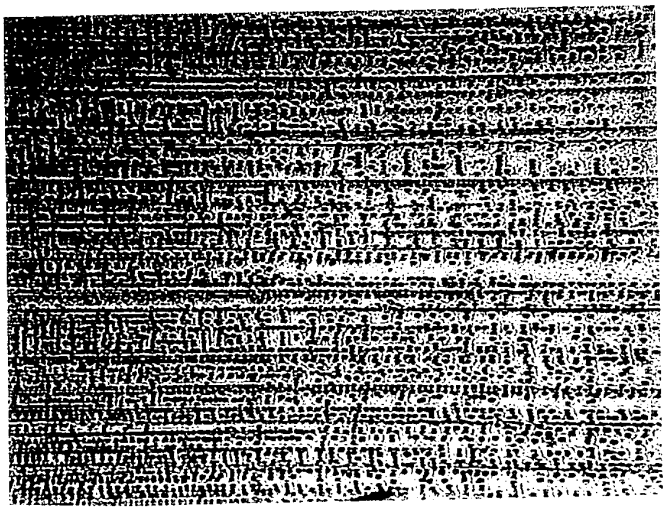

(b) Specimen 4C-3 150X

Areas on the $(10\bar{1}0)$ Prism Planes of Specimens After Creep Testing

Figure 16.

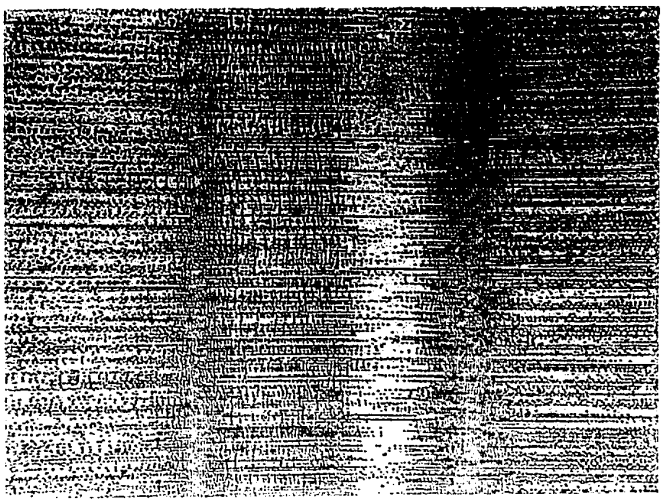

(a) Specimen 3C-4 100X $(10\bar{1}0)$ —— $< \bar{1}2\bar{1}0 >$

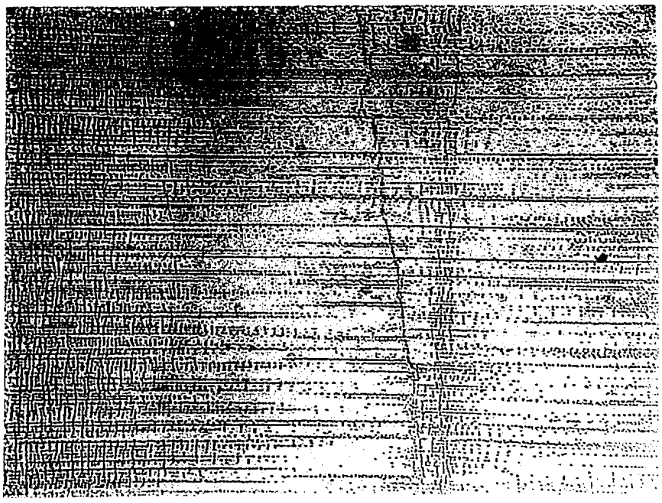

(b) Specimen 3C-4 100X

Areas on the $(10\bar{1}0)$ Prism Plane of a Specimen After Creep Testing.

Figure 17.

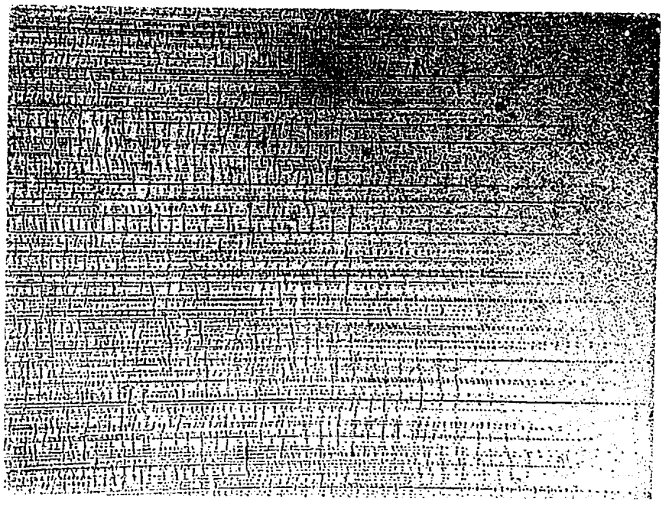

(a) Specimen 3C-4. Opposite Face of Figure 17 X100

$(10\bar{1}0)$

$\longrightarrow \langle \bar{1}2\bar{1}0 \rangle$

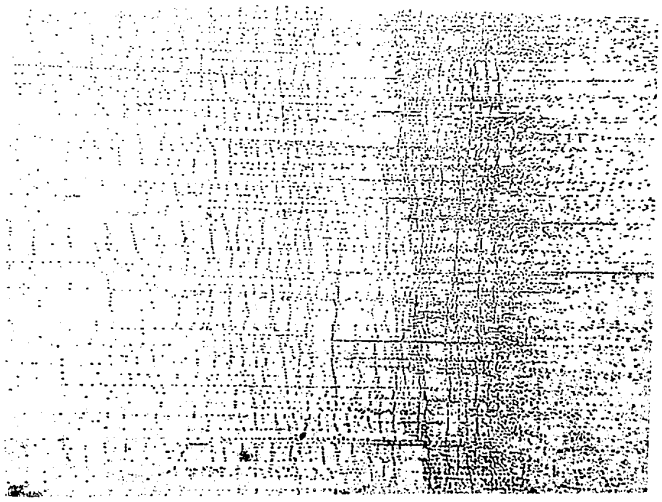

(b) Specimen 3C-4. Opposite Face of Figure 17 X100

Areas on the $(10\bar{1}0)$ Prism Plane of a Specimen After Creep Testing.

Figure 18.

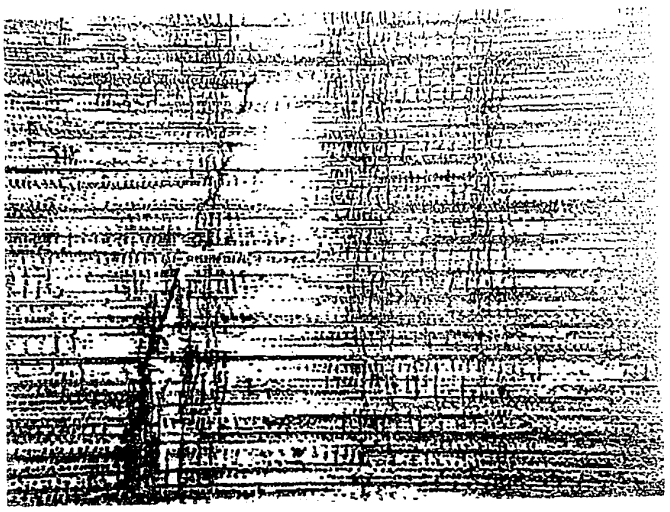

(a) Specimen 4C-4 100X

$(10\bar{1}0)$

—— $< \bar{1}2\bar{1}0 >$

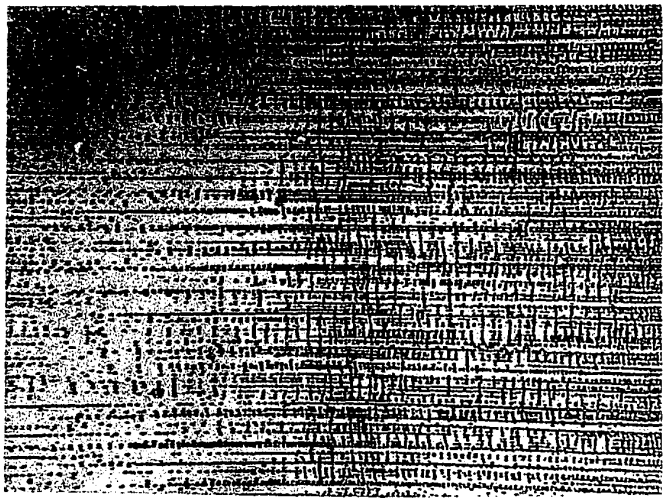

(b) Specimen 4C-4 100X

Areas on the $(10\bar{1}0)$ Prism Plane of a Specimen After Creep Testing.

Figure 19.

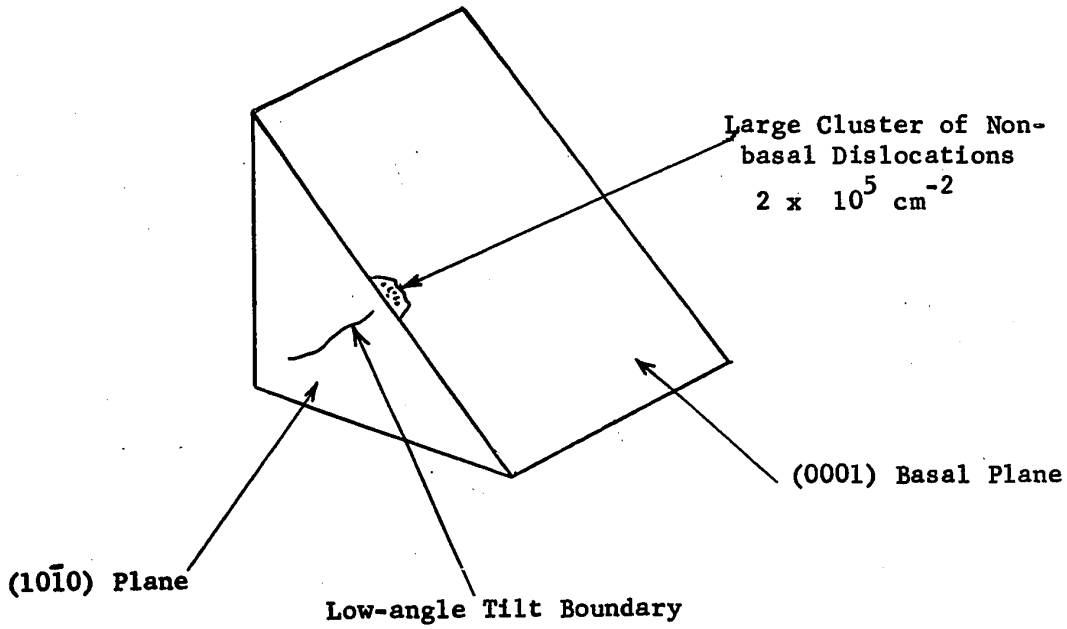

Cluster of Non-basal Dislocations on Basal Plane
Near Intersection of Tilt Boundary on (10$\bar{1}$0) Plane.

Figure 20.

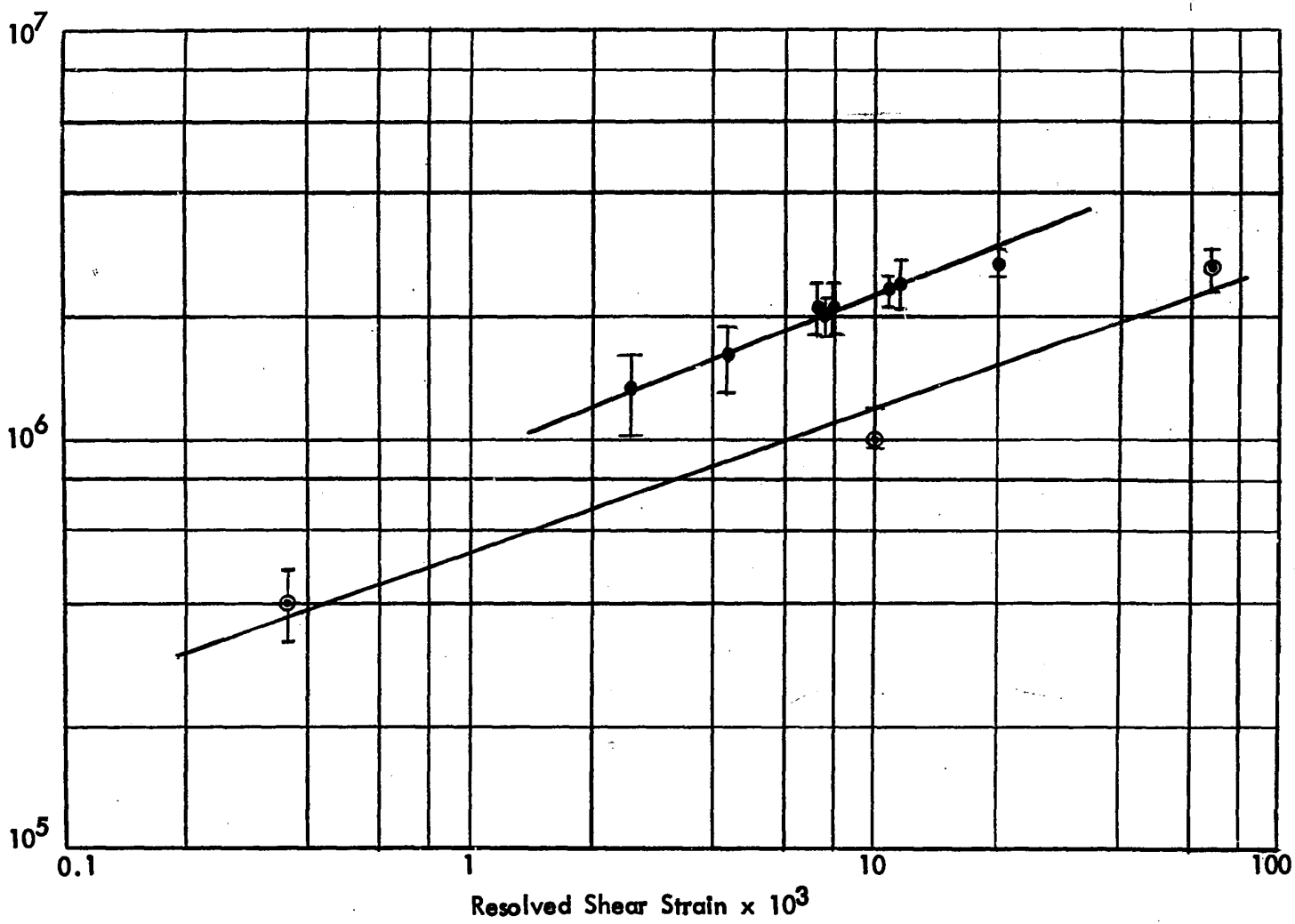

● Measurements of Present Author

◉ Measurements of Adams et al (1965a)

Change in Basal Dislocation Density Versus Resolved Shear Strain for Basal Slip

Figure 21.

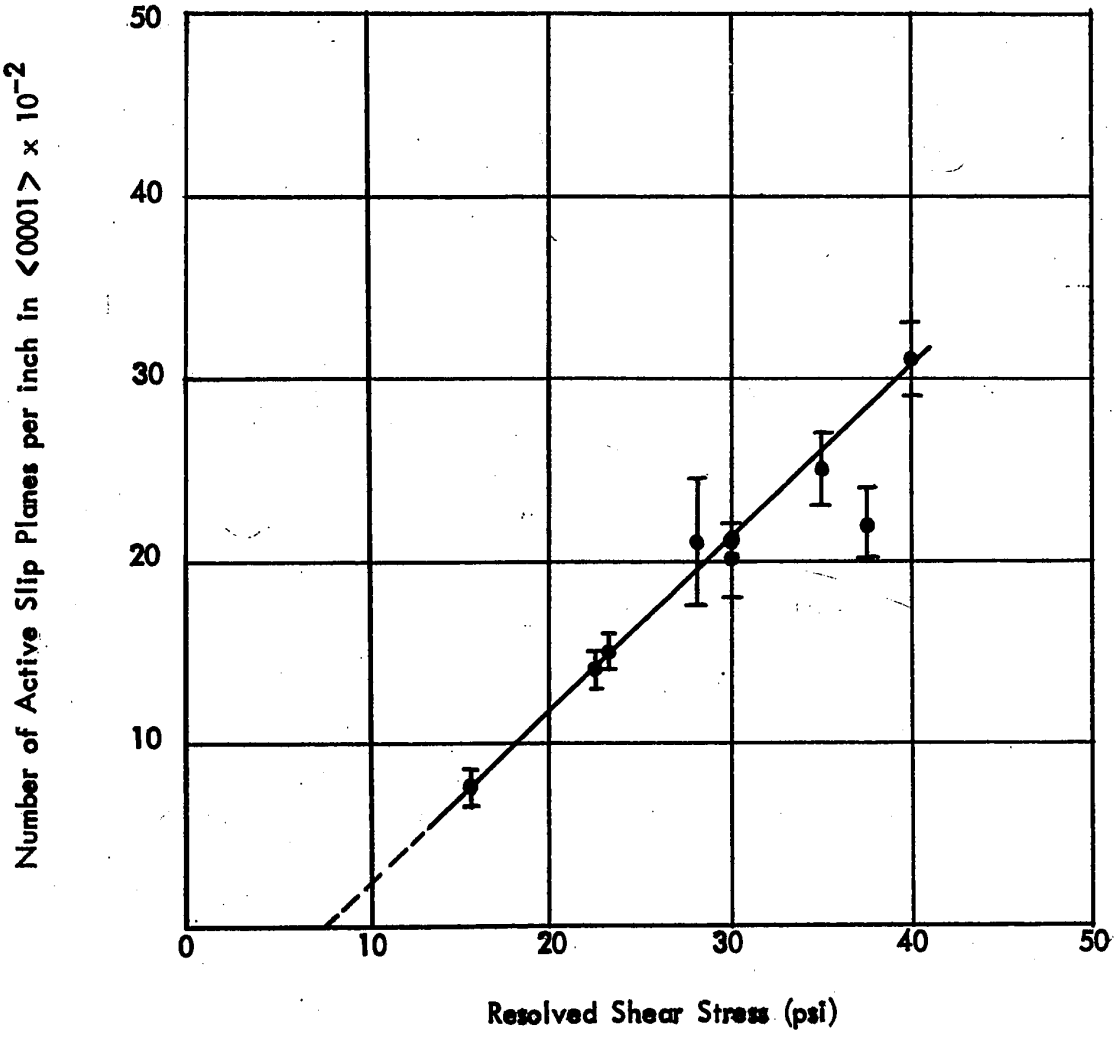

Number of Active Slip Planes Versus Resolved Shear Stress for Basal Slip

Figure 22

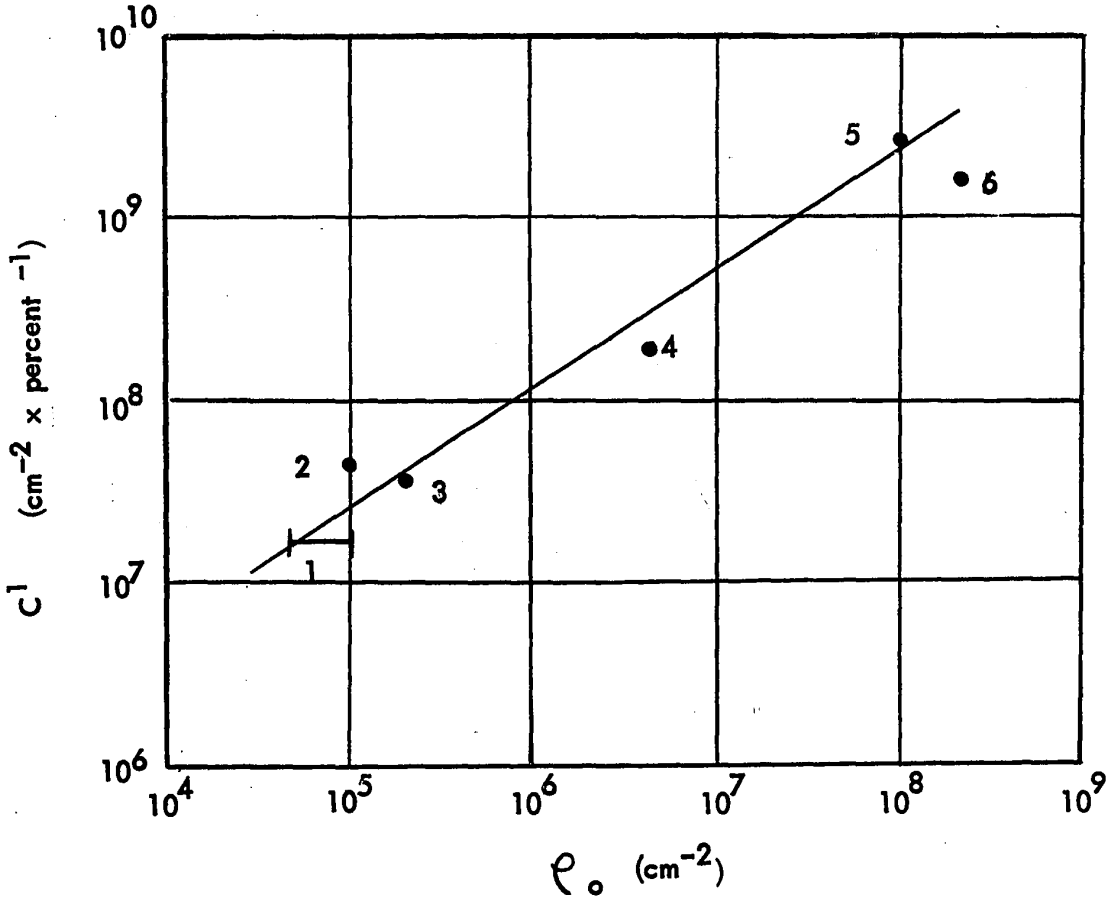

Variation of the Linear Average Value of C^1 with the Density of Grown-in Dislocations for Single Crystals in the Easy Glide Region.

1	Adams et al (1965a) - Zinc
2	Hordon (1962) - Copper
3	Present author - Zinc
4 , 5	Levinstein and Robinson (1963) - Silver
6	Hirsch (1965) - Magnesium

Figure 23.

BIBLIOGRAPHY

1. ADAMS, K.H., VREELAND, T. Jr., WOOD D.S. (1965a)
"Impurity Effects on Basal Slip in Zinc",
California Institute of Technology Research Report
CALT 473-5.

2. ADAMS, K.H., VREELAND, T. Jr., WOOD, D.S. (1965b),
"Basal Dislocation Mobility in High Purity Zinc
Single Crystals",
California Institute of Technology Research Report
CALT 473-4.

3. AXELRAD, D.R. (1962),
"A High Temperature Furnace for Studies of the
Mechanical Properties of Materials up to 2100°C",
Journal of Scientific Instruments, 39, 640.

4. AXELRAD, D.R. (1965),
"A New High Temperature Materials Testing Apparatus",
Proceedings of The Institute of Mechanical Engineers
(London), 14, 348.

5. BOWEN and CHRISTIAN (1965),
"The Calculation of Shear Stress and Shear Strain for
Double Glide in Tension and Compression",
Philosophical Magazine, 12, 369.

6. BRANDT, R.C., ADAMS, K.H., VREELAND, T. Jr., (1963),
"Etching of High Purity Zinc",
Journal of Applied Physics, 34, 3, 587.

7. BROWN, A.F. (1952),
"Surface Effects in Plastic Deformation of Metals",
Advances in Physics, 1, 4, 427.

8. CONRAD, H. (1961),
"Experimental Evaluation of Creep and Stress Rupture",
Mechanical Behaviour of Materials at Elevated Temper-
atures (Editor: Dorn), McGraw Hill, N.Y.

9. CONRAD, H., ROBERTSON, W.D. (1957),
"Effect of Temperature on the Flow Stress and Strain-
Hardening Coefficient of Magnesium Single Crystals",
Transactions of the AIME, 209, 503

10. CONRAD, H., ROBERTSON, W.D. (1958),
"Creep Characteristics of Magnesium Single Crystals
from 78° to 364°K",
Transactions of the AIME, 212, 536.

11. CONRAD, H., HAYS, L., SCHOECK, G., WIEDERSICH, H., (1961), "On the Rate-Controlling Mechanism for Plastic Flow of Mg Crystals at Low Temperatures", Acta Metallurgica, 9, 367.

12. COTTRELL, A.H. (1952-1953), Journal of the Mechanics and Physics of Solids, 1, 53.

13. COTTRELL, A.H. (1953), "Dislocations and Plastic Flow in Crystals", Oxford University Press, London, 199.

14. COTTRELL, A.H., AYTEKIN, V. (1950), "The Flow of Zinc Under Constant Stress", The Journal of the Institute of Metals, 77, 389.

15. FRIEDEL, (1963), "On the Elastic Limit of Crystals", Electron Microscopy and Strength of Crystals, Interscience, N.Y., 605.

16. FRIEDEL, J. (1964) Dislocations, Pergamon Press, London, 303.

17. GILMAN, J.J. (1956) "Plastic Anisotropy of Zinc Monocrystals", Transactions of the AIME, 206, 1326.

18. HIRSCH, P.B., LALLY, J.S. (1965), "The Deformation of Magnesium Single Crystsls", Philosophical Magazine, 12, 595.

19. HORDON, M.J. (1962), "Dislocation Density and Flow Stress of Copper", Acta Metallurgica, 10, 999.

20. JOHNSTON, W.G., GILMAN, J.J. (1959), "Dislocation Velocities, Dislocation Densities and Plastic Flow in Lithium Fluoride Crystals", Journal of Applied Physics, 30, 129.

21. LEVINSTEIN, H.J., ROBINSON, W.H. (1963), "Dislocation Configuration in Deformed Silver Single Crystals", The Relation Between the Structure and Mechanical Properties of Metals, Her Majesties Stationery Office, London, 180.

22. LIVINGSTON, J.D. (1962)
"The Density and Distribution of Dislocations in Deformed Copper Crystals",
Acta Metallurgica, 10, 299.

23. MOTT, N.F. (1952),"A Theory of Work Hardening of Metal Crystals",
Philosophical Magazine, 43, 1151.

24. REID, C.N., GILBERT, A., ROSENFIELD, A.R. (1965),
"Dislocation Multiplication",
Philosophical Magazine, 12, 409.

25. ROSENBAUM, H.S. (1961),
"Non-Basal Slip and Twin Accommodation in Zinc Crystals",
Acta Metallurgica, 9, 742

26 ROSENBAUM, H.S., SAFFREN, M.M., (1961),
"Dislocation Etch Pits on the Basal Plane of Zinc Crystals",
Journal of Applied Physics, 32, 10, 1866.

27. SAADA, G. (1960),"On the Interaction between a Fixed Dislocation and a Mobile Dislocation in Its Slip Plane",
Acta Metallurgica, 8, 200.

28. SCHOECK, G. (1961), "Theories of Creep",
Mechanical Behaviour of Materials at Elevated Temperatures (Editor: Dorn), McGraw Hill N.Y., 79.

29. SEEGER, A. (1957),"The Mechanism of Glide and Work Hardening in Face-Centred Cubic and Hexagonal Close-Packed Metals",
Dislocations and Mechanical Properties of Crystals (Editors: Fisher, Johnston, Thomson and Vreeland),
John Wiley, N.Y. 243.

30. SINHA, P.P., BECK, P.A. (1961),
"Polygonization in Bent Zinc Crystals",
Journal of Applied Physics, 32, 7, 1222.

31. SLIFKIN, L., KAUZMANN, W. (1952),
"The Creep of Zinc Single Crystals",
Journal of Applied Physics, 23, 7, 746.

32. TAYLOR, G.I. (1934),
"The Mechanism of Plastic Deformation of Crystals",
Proceedings of the Royal Society, A, 145, 362.